Measurement of the cross section for top quark pair production in association with a W or Z boson in proton-proton collisions at $\sqrt{s} = 13$ TeV

CMS Collaboration ; Canelli, Maria Florencia ; Kilminster, Benjamin ; Aarrestad, Thea K ; Brzhechko, Danyyl ; Caminada, Lea ; De Cosa, Annapaoloa ; Del Burgo, Riccardo ; Donato, Silvio ; Galloni, Camilla ; Hreus, Tomas ; Leontsinis, Stefanos ; Mikuni, Vinicius Massami ; Neutelings, Izaak ; Rauco, Giorgia ; Robmann, Peter ; Salerno, Daniel ; Schweiger, Korbinian ; Seitz, Claudia ; Takahashi, Yuta ; Wertz, Sebastien ; Zucchetta, Alberto ; et al

Abstract: A measurement is performed of the cross section of top quark pair production in association with a W or Z boson using proton-proton collisions at a center-of-mass energy of 13 TeV at the LHC. The data sample corresponds to an integrated luminosity of $35.9 fb^1$, collected by the CMS experiment in 2016. The measurement is performed in the same-sign dilepton, three- and four-lepton final states. The production cross sections are measured to be $\sigma\left(\mathrm{t\bar{t}Z}\right) = 0.99^{+0.09}_{-0.08}(\mathrm{stat})^{+0.12}_{-0.10}\,(\mathrm{syst})$ pb. The expected (observed) signal significance for the $t\bar{t}W$ production in same-sign dilepton channel is found to be 4.5 (5.3) standard deviations, while for the $t\bar{t}Z$ production in three- and four-lepton channels both the expected and the observed significances are found to be in excess of 5 standard deviations. The results are in agreement with the standard model predictions and are used to constrain the Wilson coefficients for eight dimension-six operators describing new interactions that would modify $t\bar{t}W$ and $t\bar{t}Z$ production.

DOI: https://doi.org/10.1007/JHEP08(2018)011

Published for SISSA by Springer

Received: November 7, 2017
Revised: June 14, 2018
Accepted: July 10, 2018
Published: August 3, 2018

Measurement of the cross section for top quark pair production in association with a W or Z boson in proton-proton collisions at $\sqrt{s} = 13$ TeV

The CMS collaboration

E-mail: cms-publication-committee-chair@cern.ch

Abstract: A measurement is performed of the cross section of top quark pair production in association with a W or Z boson using proton-proton collisions at a center-of-mass energy of 13 TeV at the LHC. The data sample corresponds to an integrated luminosity of 35.9 fb^{-1}, collected by the CMS experiment in 2016. The measurement is performed in the same-sign dilepton, three- and four-lepton final states. The production cross sections are measured to be $\sigma(\text{t}\bar{\text{t}}\text{W}) = 0.77^{+0.12}_{-0.11}(\text{stat})^{+0.13}_{-0.12}(\text{syst})$ pb and $\sigma(\text{t}\bar{\text{t}}\text{Z}) = 0.99^{+0.09}_{-0.08}(\text{stat})^{+0.12}_{-0.10}(\text{syst})$ pb. The expected (observed) signal significance for the $\text{t}\bar{\text{t}}\text{W}$ production in same-sign dilepton channel is found to be 4.5 (5.3) standard deviations, while for the $\text{t}\bar{\text{t}}\text{Z}$ production in three- and four-lepton channels both the expected and the observed significances are found to be in excess of 5 standard deviations. The results are in agreement with the standard model predictions and are used to constrain the Wilson coefficients for eight dimension-six operators describing new interactions that would modify $\text{t}\bar{\text{t}}\text{W}$ and $\text{t}\bar{\text{t}}\text{Z}$ production.

Keywords: Hadron-Hadron scattering (experiments), Top physics

ArXiv ePrint: 1711.02547

https://doi.org/10.1007/JHEP08(2018)011

JHEP08(2018)011

Contents

JHEP08(2018)011

1 Introduction

The 13 TeV center-of-mass energy of proton-proton (pp) collisions at the LHC opens the possibility for studying the processes at larger mass scales than previously explored in the laboratory. The top quark-antiquark pair ($\text{t}\bar{\text{t}}$) produced in association with a W ($\text{t}\bar{\text{t}}\text{W}$) or Z ($\text{t}\bar{\text{t}}\text{Z}$) boson is among the most massive signatures that can be studied with high precision. The theoretical cross sections at next-to-leading order (NLO) in quantum chromodynamics (QCD) for $\text{t}\bar{\text{t}}\text{W}$ and $\text{t}\bar{\text{t}}\text{Z}$ production at $\sqrt{s} = 13$ TeV are about 3–4 times higher than those at 8 TeV [1]. This, coupled with the higher integrated luminosity collected at 13 TeV collisions, allows for a much more accurate study of these processes. Precise measurements of the production cross section for $\text{t}\bar{\text{t}}\text{W}$ and $\text{t}\bar{\text{t}}\text{Z}$ are of particular interest because these topologies can receive sizeable contributions from new physics (NP) beyond the standard model (SM) [2, 3]. Furthermore, these processes form dominant backgrounds to several

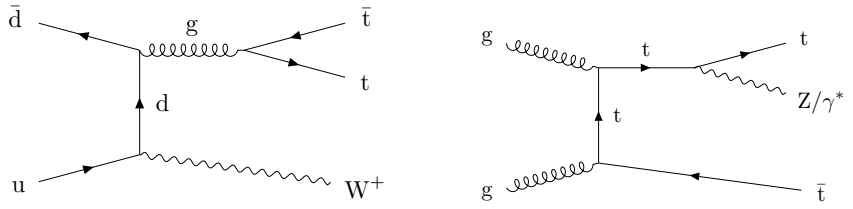

Figure 1. Representative leading-order Feynman diagrams for $t\bar{t}W$ and $t\bar{t}Z$ production at the LHC.

searches for NP, as well as to the measurements of SM processes, such as $t\bar{t}$ production in association with the Higgs boson ($t\bar{t}H$). In addition, $t\bar{t}Z$ production is the most sensitive process for directly measuring the coupling of the top quark to the Z boson. The Feynman diagrams for the dominant production mechanisms of these processes are shown in figure 1, to which the charge-conjugate states should be added.

The $t\bar{t}Z$ cross section was measured by the CMS collaboration at $\sqrt{s} = 7\,\text{TeV}$ with a precision of $\approx 50\%$ [4]. At $\sqrt{s} = 8\,\text{TeV}$ CMS used multivariate techniques in events containing two, three, or four charged leptons to measure the $t\bar{t}W$ and $t\bar{t}Z$ cross sections with a precision of 30 and 25%, respectively [5, 6]. The $t\bar{t}Z$ process was observed with a significance of 6.4 standard deviations, and evidence for $t\bar{t}W$ production was found with a significance of 4.8 standard deviations. The ATLAS Collaboration analyzed events containing two and three charged leptons for its $t\bar{t}W$ measurement, and using two, three, and four charged leptons for the $t\bar{t}Z$ channel, achieving a similar precision [7]. In a more recent publication, the ATLAS Collaboration reported the first measurement of the $t\bar{t}W$ and $t\bar{t}Z$ production cross sections at $\sqrt{s} = 13\,\text{TeV}$ [8] with a significantly smaller data set than the one considered here.

In this paper we present measurements of the $t\bar{t}Z$ and $t\bar{t}W$ production cross sections at $\sqrt{s} = 13\,\text{TeV}$ with a data set corresponding to an integrated luminosity of $35.9\,\text{fb}^{-1}$. The measurements are performed using events in which at least one of the W bosons, originating from a top quark decay, further decays to a charged lepton and a neutrino, and the associated W or Z boson decays to a charged lepton and a neutrino or a charged lepton pair, where the charged lepton (ℓ) refers to an electron or a muon. The contribution from τ leptons are included through their decays to electrons and muons. The analysis is performed in three exclusive final states, in which events with two leptons of same charge, denoted as same-sign (SS) dileptons, are used to extract the $t\bar{t}W$ signal, while events with three or four charged leptons that include a lepton pair of opposite charge and same flavor (OSSF) are used to measure the $t\bar{t}Z$ signal yield. In addition to the individual $t\bar{t}W$ and $t\bar{t}Z$ cross section measurements, a fit is performed in all three final states to simultaneously extract these cross sections. Furthermore, the results are interpreted in the context of an effective field theory to constrain the Wilson coefficients [9], which parameterize the strength of new physics interactions, for a set of selected dimension-six operators that might signal the presence of NP contributions in $t\bar{t}W$ and $t\bar{t}Z$ production.

JHEP08(2018)011

2 The CMS detector

The central feature of the CMS apparatus is a superconducting solenoid of 6 m internal diameter, providing a magnetic field of 3.8 T. Within the solenoid volume are a silicon pixel and strip tracker, a lead tungstate crystal electromagnetic calorimeter (ECAL), and a brass and scintillator hadron calorimeter (HCAL), each composed of a barrel and two endcap sections. Forward calorimeters extend the pseudorapidity (η) coverage provided by the barrel and endcap detectors. Muons are detected in gas-ionization chambers embedded in the steel magnetic flux-return yoke outside the solenoid. A more detailed description of the CMS detector, together with a definition of the coordinate system used and the relevant kinematic variables, can be found in ref. [10]. Events of interest are selected using a two-tiered trigger system [11]. The first level, composed of custom hardware processors, uses information from the calorimeters and muon detectors to select events, while the second level selects events by running a version of the full event reconstruction software optimized for fast processing on a farm of computer processors.

3 Event and object selection

Events are selected by online triggers that require the presence of at least one electron or muon, with transverse momentum, p_{T}, greater than 27 or 24 GeV, respectively. The selection efficiencies for the signal and background events that pass all requirements are found to be greater than 95 and 98% for the dilepton analysis and for the three- and four-lepton analyses, respectively.

The Monte Carlo (MC) simulations are used to estimate some of the backgrounds, as well as to calculate the selection efficiencies for the $\mathrm{t\bar{t}Z}$ and $\mathrm{t\bar{t}W}$ signal events. The simulated events for the $\mathrm{W}\gamma^*$, WW, tWZ, and for pairs of top quarks associated with a pair of bosons ($\mathrm{t\bar{t}VV}$, where V = W, Z, or H) processes, are performed at leading order (LO) in QCD, and for $\mathrm{t\bar{t}Z}$, $\mathrm{t\bar{t}W}$, tZq, tHq, tHW, WZ, WWZ, WZZ, ZZZ, $\mathrm{t\bar{t}}\gamma^*$, and $\mathrm{Z}\gamma^*$ final states at NLO in QCD using the MadGraph5_aMC@NLO v2.2.2 or v2.3.3 [12]. The NLO powheg v2 [13] generator is used for the production of the $\mathrm{t\bar{t}H}$ [14] and $\mathrm{q\bar{q}}\rightarrow$ ZZ [15, 16] processes, while the gg $\rightarrow$ ZZ process is generated at LO in QCD with mcfm v7.0 [17]. The simulated samples of ZZ events are scaled to the cross sections calculated at next-to-next-to-leading order (NNLO) in QCD for $\mathrm{q\bar{q}} \rightarrow$ ZZ [18] (using a scaling K factor of 1.1) and for gg $\rightarrow$ ZZ at NLO [19] (using $K = 1.7$). The NNPDF3.0LO [20] parton distribution functions (PDFs) are used for the simulation generated at LO and the NNPDF3.0NLO [20] PDF for those generated at NLO. Parton showering, hadronization, and the underlying event are simulated using pythia v8.212 [21, 22] with the CUETP8M1 tune [23, 24]. The double counting of the partons generated with MadGraph5_aMC@NLO and those with pythia is removed using the MLM [25] and the FxFx [26] matching schemes, in the LO and NLO generated events, respectively. All events are processed through a simulation of the CMS detector based on Geant4 [27] and are reconstructed with the same algorithms as used for data. Simultaneous pp collisions in the same or nearby bunch crossings, referred to as pileup (PU), are also simulated. The PU distribution used in simulation is chosen to match the one observed in the data.

JHEP08(2018)011

The theoretical cross sections for the $t\bar{t}W$ and $t\bar{t}Z$ signal processes are computed at NLO in QCD using MadGraph5_aMC@NLO and found to be 0.628 ± 0.082 and 0.839 ± 0.101 pb [1], respectively. These values are used to normalize the expected signal yields, as well as to rescale the measured signal strengths to obtain the final cross sections. In the calculation for $t\bar{t}Z$, the cross section corresponds to a phase space where the invariant mass of all pairs of leptons is required to be greater than 10 GeV.

Event reconstruction uses the CMS particle-flow (PF) algorithm [28] for particle reconstruction and identification. Because of PU, there can be far more than one collision vertex reconstructed per event. The reconstructed vertex for which the sum of the p_T of the physics objects is largest is chosen to be the primary pp interaction vertex. The physics objects here are the objects obtained by a jet finding algorithm [29, 30] applied to all charged tracks associated with this vertex, plus the missing transverse momentum (p_T^{miss}), which is computed as the magnitude of the vector sum of the p_T of all PF candidates.

Leptons are required to have $p_T > 10$ GeV and $|\eta| < 2.5\,(2.4)$ for electrons (muons) and must be isolated from the other particles produced in the collision. A relative isolation parameter, I_{rel}, is determined by a cone-based algorithm. For each electron (muon) candidate, a cone of $\Delta R = \sqrt{(\Delta\eta)^2 + (\Delta\phi)^2} = 0.3\,(0.4)$ is constructed around the track direction at the event primary vertex, where $\Delta\eta$ and $\Delta\phi$ are the respective differences in pseudorapidity and azimuthal angle (in radians) relative to the lepton track. The scalar sum of the p_T of all PF particles within this cone is calculated, excluding the lepton candidate and any charged particle not originating from the selected primary vertex. Exclusion of such particles removes the PU contribution from the charged particles, and a correction is therefore still required for the neutral component. The average energy density deposited by neutral particles in the event, computed with the FastJet [30, 31] program, is therefore subtracted from the neutral component to the sum of the p_T of particles in the cone. The quantity I_{rel} is then defined as the ratio of this corrected sum to the p_T of the lepton candidate. An electron candidate is selected if $I_{rel} < 0.1$ for all three analyses, while a muon candidate is selected if $I_{rel} < 0.25$ for the three- and four-lepton analyses, and if $I_{rel} < 0.15$ for the SS dilepton analysis. Consistency of the origination of the lepton from the primary vertex is enforced by requiring lepton transverse and longitudinal displacements from the primary vertex to be less than 0.05 and 0.1 cm, respectively. Additionally, the transverse impact parameter is required to be smaller than 4 standard deviations, where the impact parameter is the minimum spatial distance between the lepton trajectory and the primary vertex.

Jets are reconstructed by clustering PF candidates using the anti-k_T algorithm [29] with a distance parameter $R = 0.4$. The influence of PU is mitigated through a charged-hadron subtraction technique, which removes the energy of charged hadrons not originating from the primary vertex [32]. Jets are calibrated in simulation, and separately in data, accounting for energy deposits of neutral particles from PU and any nonlinear detector response. Calibrated jets with $p_T > 30$ GeV and $|\eta| < 2.4$ are selected for the analysis. Furthermore, jets formed with fewer than three PF candidates or with electromagnetic or hadronic energy fractions greater than 99% are vetoed. A selected jet can also overlap with selected leptons and lead thereby to some double counting. To prevent such cases, jets that are found within a cone of $\Delta R = 0.4$ around any of the signal leptons are removed from consideration.

JHEP08(2018)011

A multivariate b tagging discriminator [33, 34] is used to identify jets that originate from the hadronization of b quarks (b jets). The selection criteria used in this analysis gives about 1% rate for tagging light-quark or gluon jets as b jets and a corresponding b tagging efficiency of around 70%, depending on the jet p_{T} and η.

4 Event selection

4.1 SS dilepton analysis

We measure the production rate of $\mathrm{t\bar{t}W}$ events in the decay channel that yields exactly two leptons with the same charge. Requiring the same electric charge for the two leptons retains only one third of the signal in the dilepton final state. However, this selection significantly improves the signal-to-background ratio, as SS lepton pairs are produced in SM processes with relatively small cross sections. The main backgrounds to this analysis originate from misreconstruction effects: misidentification of leptons from heavy-quark decays, hereafter called nonprompt leptons to distinguish them from prompt leptons originating from W and Z boson decays, and mismeasurement of the charge of one of the leptons in events with an oppositely charged lepton pair.

We select events with two SS leptons ($\mu\mu$, μe, ee), requiring the p_{T} of both leptons to be above 25 GeV. To avoid inefficiencies due to the trigger selection in the ee channel, the electron with higher p_{T} is required to have $p_{\mathrm{T}} > 40$ GeV. Events containing additional leptons passing looser identification and isolation requirements are vetoed. These loose identification and isolation criteria are the same as used to estimate the nonprompt background in data (see section 5). The invariant mass of the two leptons must be greater than 12 GeV to suppress Drell–Yan (DY) and quarkonium processes. To suppress $\mathrm{Z} \to \mathrm{e^+e^-}$ events, the invariant mass of the two electrons is required to lie outside the 15 GeV window around the Z boson mass $M(\mathrm{Z})$ [35], followed by the requirement that $p_{\mathrm{T}}^{\mathrm{miss}} > 30$ GeV.

In order to distinguish these backgrounds from the signal, a multivariate analysis (MVA) has been developed. The MVA has been trained using the $\mathrm{t\bar{t}W}$ signal and the main background process, using events with at least two jets, one or more of which are identified as b jets. Among the observables examined as inputs to the MVA training, the following are found to provide the best discrimination between the signal and background: the number of jets, N_{j}, the number of b jets, N_{b}, the scalar sum of p_{T} of the jets, H_{T}, $p_{\mathrm{T}}^{\mathrm{miss}}$, the highest-$p_{\mathrm{T}}$ (leading) and the lowest-p_{T} (trailing) lepton p_{T}, the invariant mass calculated using $p_{\mathrm{T}}^{\mathrm{miss}}$ and p_{T} of each lepton, M_{T}, the leading and next-to-highest-p_{T} (subleading) jet p_{T}, and the separation ΔR between the trailing lepton and the nearest selected jet.

A boosted decision tree classifier with gradient boosting [36] is used as the MVA discriminant, and simulated events are split into equal training and testing samples. Figure 2 shows the kinematic distributions of variables used in the MVA, and figure 3 displays the output of the boosted decision tree classifier (D) for all background sources and the signal, scaled to the integrated luminosity of the analyzed data samples.

Events with $D > 0$ are selected to suppress the background from nonprompt leptons, and, for final signal extraction, they are split into two categories: $0 < D < 0.6$ and $D > 0.6$. These values are optimized to achieve the best expected sensitivity for $\mathrm{t\bar{t}W}$. Furthermore,

JHEP08(2018)011

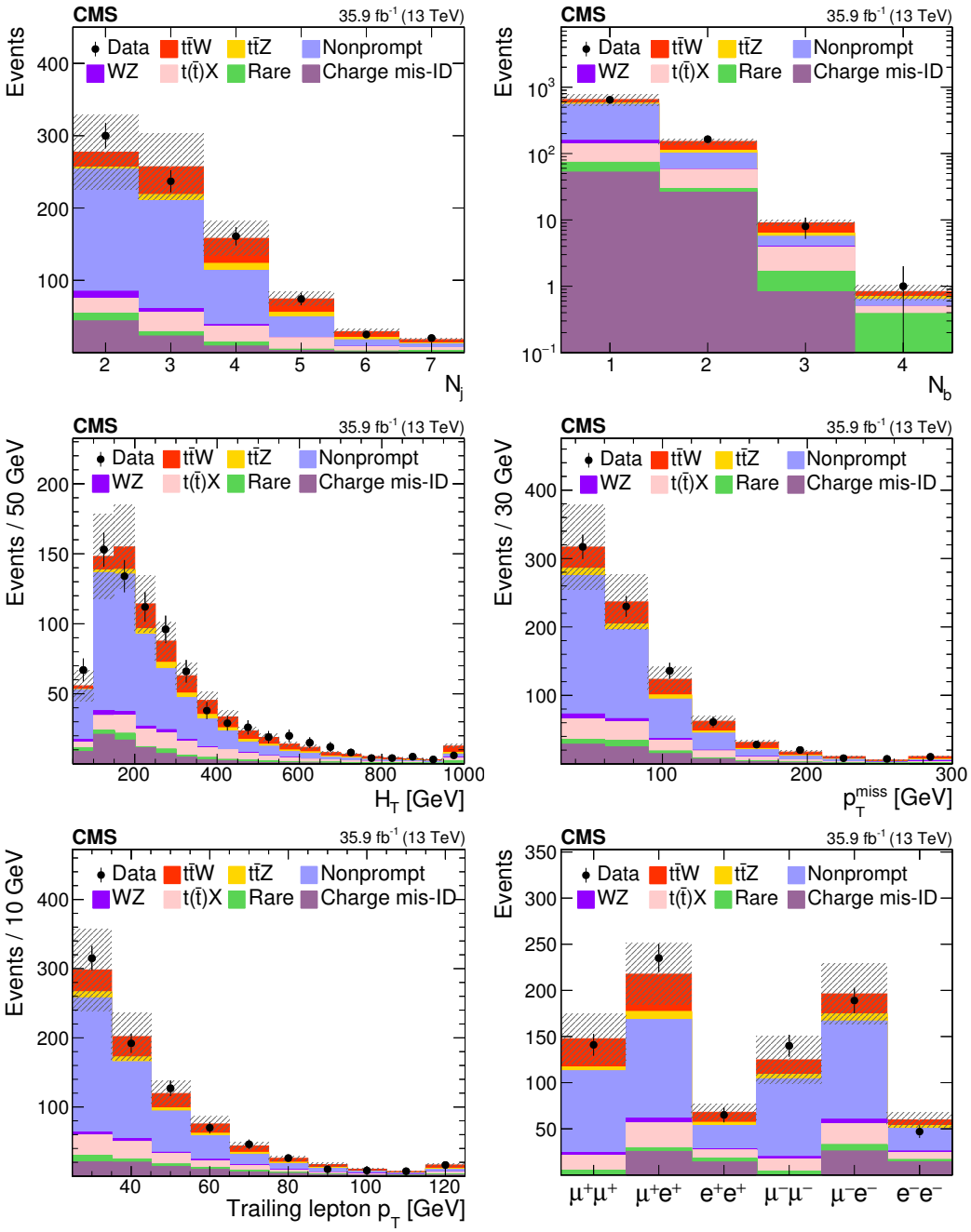

Figure 2. Distributions of different variables in data from the SS dilepton analysis, compared to the MC generated expectations. From left to right: jet and b jet multiplicity (upper), H_T and p_T^{miss} (center), trailing lepton p_T and event yields in each lepton-flavor combination (lower). The expected contributions from the different background processes are stacked, as well as the expected contribution from the signal. The shaded band represents the total uncertainty in the prediction of the background and the signal processes. See section 5 for the definition of each background category.

JHEP08(2018)011

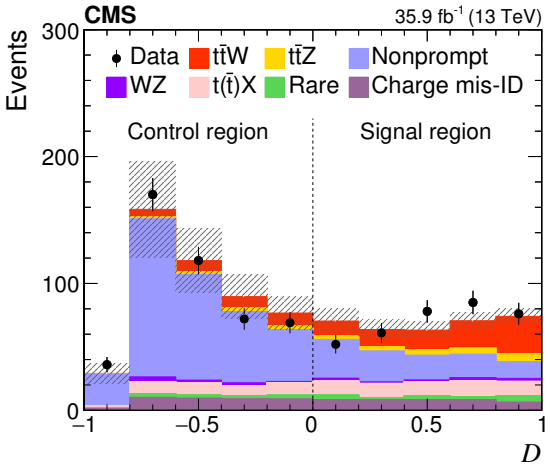

Figure 3. Distribution of the boosted decision tree classifier D for background and signal processes in the SS dilepton analysis. The expected contribution from the different background processes, and the signal as well as the observed data are shown. The shaded band represents the total uncertainty in the prediction of the background and the signal processes. See section 5 for the definition of each background category.

the number of jets and b jets are also used to form five exclusive event categories that maximize signal significance. The categories are formed using events with $N_{\mathrm{j}} = 2$, 3, and >3. The latter two categories are further split according to the number of b jets, $N_{\mathrm{b}} = 1$ and $N_{\mathrm{b}} > 1$. Events with $D < 0$ are also used in the signal extraction procedure to constrain the uncertainties in the nonprompt lepton background.

Each of these categories is further split into two sets according to the total charge of the leptons: $\ell^+\ell^+$ or $\ell^-\ell^-$. This increases the sensitivity to the charge-asymmetric production of the signal ($\mathrm{t\bar{t}W^+}$ vs. $\mathrm{t\bar{t}W^-}$) resulting from the pp nature of the collision at the LHC, while the main backgrounds yield charge-symmetric dileptons. In total, we form 20 exclusive signal regions.

4.2 Three-lepton analysis

The production rate of $\mathrm{t\bar{t}Z}$ events is measured in the final state with three leptons.

We select events that contain exactly three leptons ($\mu\mu\mu$, $\mu\mu$e, μee, or eee), requiring the leading, subleading, and trailing lepton p_{T} to be above 40, 20, and 10 GeV, respectively. To reduce backgrounds from multilepton processes that do not contain a Z boson, we require at least one OSSF lepton pair with invariant mass, $M(\ell\ell)$, consistent with the Z boson hypothesis, namely $|M(\ell\ell) - M(\mathrm{Z})| < 10\,\mathrm{GeV}$.

Signal events are expected to have at least four jets, two of which originate from b quarks. When the events pass the jet and b jet requirements defined in the previous section, one obtains a sample of events enriched in signal, with minimal background contribution. However, nearly 70% of the signal events fail the requirement of having four jets with two of them identified as b jets. We therefore make use of lower jet and b jet multiplicities to form nine exclusive event categories to include a larger fraction of the signal events. These

JHEP08(2018)011

nine categories are formed using events with $N_j = 2$, 3, and > 3, where each jet multiplicity gets further split according to the b jet multiplicity, $N_b = 0$, 1, and > 1.

Despite the larger background contamination, the $N_j = 3$ categories, especially in bins with larger N_b, improve the signal sensitivity, as this category recovers signal efficiency for the jets that fall outside the acceptance. The $N_j = 2$ category provides a background-dominated region that helps to constrain the background uncertainties. We use all nine signal regions to extract the signal significance and the cross section.

4.3 Four-lepton analysis

In addition to the three-lepton final state, events with four leptons are exclusively analyzed for the measurement of the $t\bar{t}Z$ production rate.

The $t\bar{t}Z$ events in this channel are characterized by the presence of two b jets, p_T^{miss}, and four leptons, two of which form an OSSF pair consistent with the Z boson mass. The event selection is optimized to obtain high signal efficiency in simulation in order to profit from low expected background yields. Events with exactly four leptons that pass the lepton identification and isolation requirements described in section 3 are selected. The leading lepton must have $p_T > 40\,\text{GeV}$ and the p_T of the remaining three leptons must exceed 10 GeV. The sum of the lepton charges must be zero, and the invariant mass of any lepton pair is required to be greater than 12 GeV. At least one OSSF lepton pair with an invariant mass $|M(\ell\ell) - M(Z)| < 20\,\text{GeV}$ must be present in the event. Events with $\mu\mu\mu\mu$, eeee, and $\mu\mu$ee final states, in which a second OSSF lepton pair consistent with the Z boson mass is found, are rejected. Events containing two jets are selected and split into two categories for signal extraction: one with zero b jets and the other with at least one b jet.

5 Background predictions

5.1 Background due to nonprompt leptons

Nonprompt leptons, i.e. leptons from heavy-flavor hadron decay, misidentified hadrons, muons from light meson decays, or electrons from unidentified photon conversions, are strongly rejected by the identification and the isolation criteria applied on electrons and muons. Nonetheless, a residual background from such leptons leaks into the analysis selection. Such backgrounds are mainly expected from $t\bar{t}$ production, in which one or two of the leptons originate from the leptonic W boson decays and an additional nonprompt lepton comes from the semileptonic decays of a b hadron, as well as from $Z \to \ell\ell$ events containing an additional misidentified lepton. These backgrounds are estimated using a data-based technique. From a control sample in data, we calculate the probability for a loosely identified nonprompt lepton to pass the full set of tight requirements, designated as the tight-to-loose ratio. For loose leptons we choose a relaxed isolation requirement, $I_{rel} < 1$, and additional electron identification requirements on the variables that distinguish prompt electrons from hadrons and photons which are misidentified as electrons. The tight-to-loose ratios are measured in a data control sample of QCD multijet events that are enriched in nonprompt leptons. This control sample consists of events with a single lepton and at least one jet, where the lepton and jets are separated by $\Delta R > 1$. We suppress

JHEP08(2018)011

the prompt lepton contamination, mostly from W+jets, by requiring $p_{\mathrm{T}}^{\mathrm{miss}} < 20\,\mathrm{GeV}$ and $M_{\mathrm{T}} < 20\,\mathrm{GeV}$, where M_{T} is the transverse mass constructed using $p_{\mathrm{T}}^{\mathrm{miss}}$ and the selected lepton. The residual prompt lepton contamination is subtracted using estimates from MC simulation. This subtraction is relevant only for the high-p_{T} leptons, and its effect on the total estimated background does not exceed a few percent. These tight-to-loose ratios are parametrized as functions of the η of the leptons and $p_{\mathrm{T}}^{\mathrm{cor}}$, with the latter calculated through corrections to lepton p_{T} as a function of the energy in the isolation cone. This definition has no impact on the p_{T} of the leptons that pass the isolation requirement, but modifies the p_{T} of those that fail, and extract thereby a more accurate value of true p_{T} [37]. The tight-to-loose ratios are then used together with the observed number of events in sideband regions. These sideband regions contain events that pass full event criteria in each analysis region, except that at least one of the leptons passes the loose selection but does not pass the tight selection. Each event in this region is assigned a weight as a function of the p_{T} and η of the loose lepton to account for the probability of the lepton to pass the tight selection.

We validate this technique using simulated events. The tight-to-loose ratios are first measured for electrons and muons in simulated multijet events, and applied in simulated $\mathrm{t\bar{t}}$ and Z+jets events in the same way as in data, to extract predictions for the nonprompt background contribution. These predictions agree very well with the observed yields in simulation, not only for the integral yields, but also for distributions in all kinematic variables used to form the analysis regions, including the boosted decision tree output D. Additionally, data control regions used in the signal-extraction regions and enriched in processes with nonprompt leptons, are formed to check any other potential sources of mismodeling. For the SS dilepton channel, we use the region with $D < 0$. Figure 4 shows the predicted background and observed data yields versus N_{j} and the p_{T} of the trailing lepton. Events in this region are also used in the signal extraction procedure for $\mathrm{t\bar{t}W}$. The potential systematic effects for the extrapolation from $D < 0$ to $D > 0$ are studied in simulation and found to be negligible compared to other sources of uncertainty. For the three-lepton channel this control region is defined by either the absence of an OSSF lepton pair, or by the presence of an OSSF, with its invariant mass being at least 10 GeV away from $M(\mathrm{Z})$, and with at least one b jet present. This region is dominated by $\mathrm{t\bar{t}}$ events in which both W bosons decay leptonically and an additional nonprompt lepton is present. Figure 5 shows the predicted and observed yields versus the flavor of the leptons, $p_{\mathrm{T}}^{\mathrm{miss}}$, N_{j}, and N_{b}. Both of these control regions show very good agreement between predicted and observed yields and for kinematic distributions that are relevant for the signal extraction.

Based on the extensive aforementioned validation in both data and simulated control samples, we conclude that a systematic uncertainty of 30% is appropriate for the prediction of the background from nonprompt leptons. The statistical uncertainties due to the limited number of observed events in the sideband regions of data are taken into account, and are often found to be larger or comparable to the systematic uncertainty.

5.2 Background induced by the mismeasurement of the lepton charge

The charge mismeasurement rate for muons is negligible and background is significant only for the channels with at least one electron. This background is estimated with a partially

JHEP08(2018)011

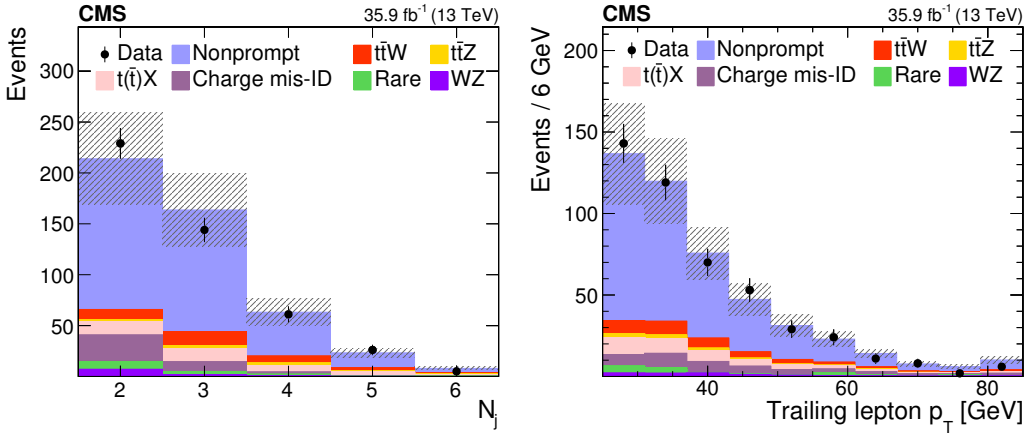

Figure 4. Distributions of the predicted and observed yields versus N_j (left) and p_T of the trailing lepton (right) in control regions enriched with nonprompt lepton background in the SS dilepton channel. The shaded band represents the total uncertainty in the prediction of the background and the signal processes. See section 5 for the definition of each background category.

data-based approach. The opposite-charge ee or eμ data events passing the full kinematic selection are weighted by the p_T- and η-dependent electron-charge misidentification probabilities. These probabilities are obtained from MC simulation. The charge mismeasurement rate in simulation is validated through a comparison with data. It is measured in DY events in MC and in data, where events are selected when the two SS electrons have an invariant mass that falls within a Z boson mass window, $76 < M(\ell\ell) < 106\,\text{GeV}$. The measured electron charge misidentification rates in data and in DY simulation are in good agreement and vary from 4×10^{-5} for low-p_T electrons in the barrel region to 4×10^{-3} for high-p_T electrons in the endcap.

The process contributing to this category of background in signal regions is primarily $t\bar{t}$ production. Based on the agreement in the charge mismeasurement rate between data and MC events, and the simulation studies of charge misidentification rate comparison between $t\bar{t}$ and DY MC events, we assign a 20% systematic uncertainty in the estimation of this background [38].

5.3 Background due to WZ production

Kinematic distributions for the background from WZ events are taken from simulation. This background has the highest expected yields in the analysis region with no b-tagged jets. The data used for this analysis contain a substantial number of WZ events that can be isolated and compared with the MC predictions. We define a control region in a subset of the data with the following requirements: we select events with three leptons, with the same p_T thresholds as the ones used in the $t\bar{t}Z$ selection, that have two leptons forming an OSSF pair with $|M(\ell\ell) - M(Z)| < 10\,\text{GeV}$, less than two jets, and no b-tagged jets. Additionally p_T^{miss} is required to be greater than 30 GeV, and M_T, constructed using this p_T^{miss} and the lepton not used in the $M(\ell\ell)$ calculation, is required to be greater than 50 GeV.

JHEP08(2018)011

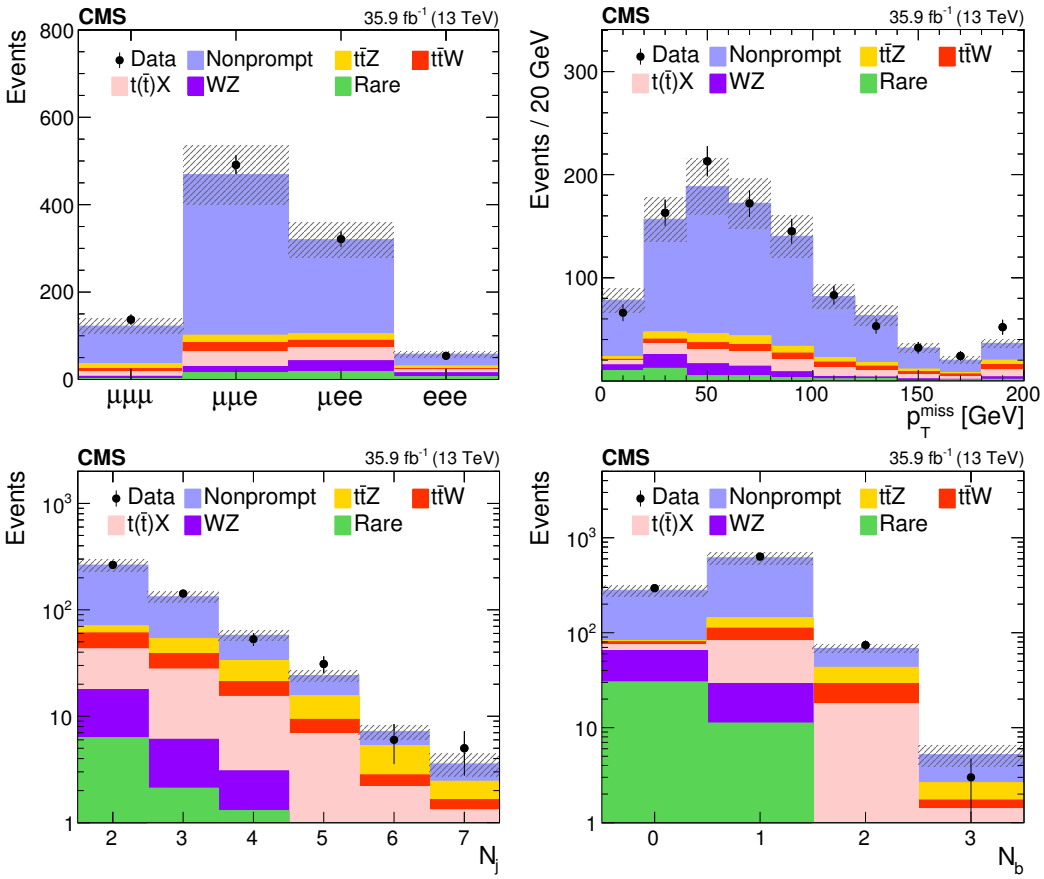

Figure 5. Distributions of the predicted and observed yields versus different three-lepton channels, $p_{\mathrm{T}}^{\mathrm{miss}}$ (upper panels), and jet and b jet multiplicity (lower panels) in control regions enriched with nonprompt lepton background. The shaded band represents the total uncertainty in the prediction of the background and the signal processes. See section 5 for the definition of each background category.

This selection provides a data sample that is expected to be 85% pure in WZ events. Figure 6 shows the number of events as a function of M_{T}, lepton flavor, N_{j}, and $M(\ell\ell)$. The expected background from nonprompt leptons is measured from data using the method described above. The other background contributions are obtained from simulation. We observe overall agreement between data and the total expectation in all four-lepton channels and also in the kinematic distributions. The ratio of the total observed yield to the predicted one is found to be 0.94 ± 0.07, where the uncertainty reflects only statistical sources. With this level of agreement between the data and MC prediction, we proceed without applying any corrections to the WZ prediction obtained from the simulation. The statistical uncertainty in the ratio is propagated to the final prediction. We also study possible mismodeling of the WZ + heavy-flavor background at large b jet multiplicities. We find that the WZ contribution at high b jet multiplicities is mainly caused by the misidentification of light-flavor jets as b jets. The fraction of WZ events containing at least one b quark is predicted by the simulation to vary between 5 and 15% across all of the

JHEP08(2018)011

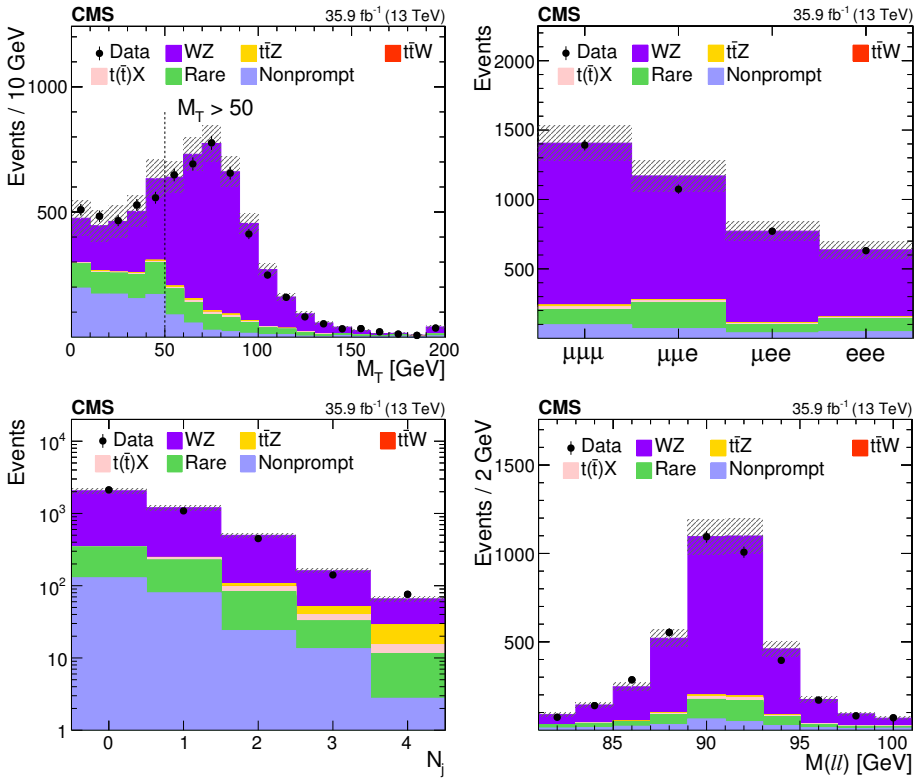

Figure 6. Distributions of the predicted and observed yields versus M_{T} (upper left), lepton flavor (upper right), jet multiplicity (lower left), and the reconstructed invariant mass of the Z boson candidates (lower right) in the WZ-enriched control region. The requirements on M_{T} and N_{j} are removed for the distributions of these variables. The shaded band represents the total uncertainty in the prediction of the background and the signal processes.

analysis categories. We apply scale factors to take into account the differences in b tagging efficiencies and misidentification probabilities between data and simulation [33, 34]. Once all the corrections are applied, we check the agreement between data and Z+jets simulated events as a function of N_{b} in OSSF dilepton events consistent with the $M(\mathrm{Z})$. Based on this study, we assign a 10% systematic uncertainty to the WZ background estimate, which covers the differences between data and expectations found in the control region. For the three-lepton analysis, an additional 20% uncertainty is introduced for regions with $N_{\mathrm{j}} > 3$. Other systematic uncertainties associated with the extrapolation from this control region to high N_{j} or N_{b} regions, such as jet energy scale and b tagging uncertainties, are considered separately.

5.4 Background due to t($\bar{\mathrm{t}}$)X and other rare SM processes

The background events containing either multiple bosons or top quark(s) in association with a W, Z, or a Higgs boson are estimated from simulation scaled by their NLO cross section and normalized to the integrated luminosity. The backgrounds that have at least one top quark in final state, i.e. t$\bar{\mathrm{t}}$H, tWZ, tqZ, tHq, tHW, t$\bar{\mathrm{t}}$VV, and t$\bar{\mathrm{t}}$t$\bar{\mathrm{t}}$, are denoted as

JHEP08(2018)011

$t(\bar{t})X$, while all others, i.e. WW, ZZ, $W\gamma^*$, $Z\gamma^*$, WWW, WWZ, WZZ, ZZZ, are grouped into the rare SM processes category.

For background yields in the $t(\bar{t})X$ category, we studied the theoretical and systematic uncertainties separately. The theoretical uncertainties for the inclusive cross section are around 10% [12, 39, 40]. Using the simulations, we study the effect of the changes made in renormalization and factorization scales (μ_R and μ_F), as well as the uncertainties from choice in PDF in the phase-space region relative to this analysis. From these studies we deduce an additional theoretical uncertainty of 2%. On the experimental side, to account for the differences in the lepton-selection efficiencies, b jet identification efficiencies, mistagging rate between the simulation and the data, we apply scale factors to the predictions obtained from simulations, and assign systematic uncertainties associated with these scale factors. These experimental uncertainties are estimated in each analysis category (see section 6) and are applied in addition to the above-mentioned 10% uncertainty in the yield.

The rate for the backgrounds from rare SM processes, except ZZ, are assigned an overall 50% systematic uncertainty. This is motivated by the fact that these processes are not yet measured at the LHC and the uncertainties associated with the absence of higher-order effects might be large in the phase-space region relevant to this analysis. For the ZZ background, the consistency between data and simulation is validated in a ZZ-dominated background region. The events are selected following the first four steps mentioned in section 4.2, in the given selection sequence, requiring two OSSF lepton pairs with an invariant mass within a 20 GeV window of $M(Z)$. The distributions of the expected and observed data yields in this ZZ enriched control region are shown in figure 7. The ZZ control region, which is better than 95% pure in ZZ events, shows good agreement between data and simulation in events with extra jets. Based on this study in the four-lepton control region, as well as considering the studies done for the WZ background at high jet multiplicities, we assign a 20% systematic uncertainty. Additional experimental uncertainties, as previously described for the $t(\bar{t})X$ and WZ backgrounds, are also applied to the ZZ background.

6 Signal acceptance and systematic uncertainties

The uncertainty in the integrated luminosity is 2.5% [41]. Simulated events are reweighted according to the distribution of the true number of interactions at each bunch crossing. The uncertainty in the total inelastic pp cross section, which affects the PU estimate, is 5% [42] and it leads to a 1–2% uncertainty in the expected yields.

We measure the trigger efficiencies in a data sample independent from the one used for the signal selection, as well as in simulation. These efficiencies are measured for each channel separately and parametrized as a function of lepton p_T and η. The overall efficiency for the SS dilepton channel is higher than 95% and that for the three- and four-lepton analyses is greater than 98%. The trigger efficiencies measured in simulation agree within 1% with the measurements in data, with an exception of the SS dimuon channel, in which the difference reaches 3%. The event yields in simulation are therefore scaled to match the trigger efficiencies in data. The systematic uncertainty due to this scaling is 2–4% depending on the channel.

JHEP08(2018)011

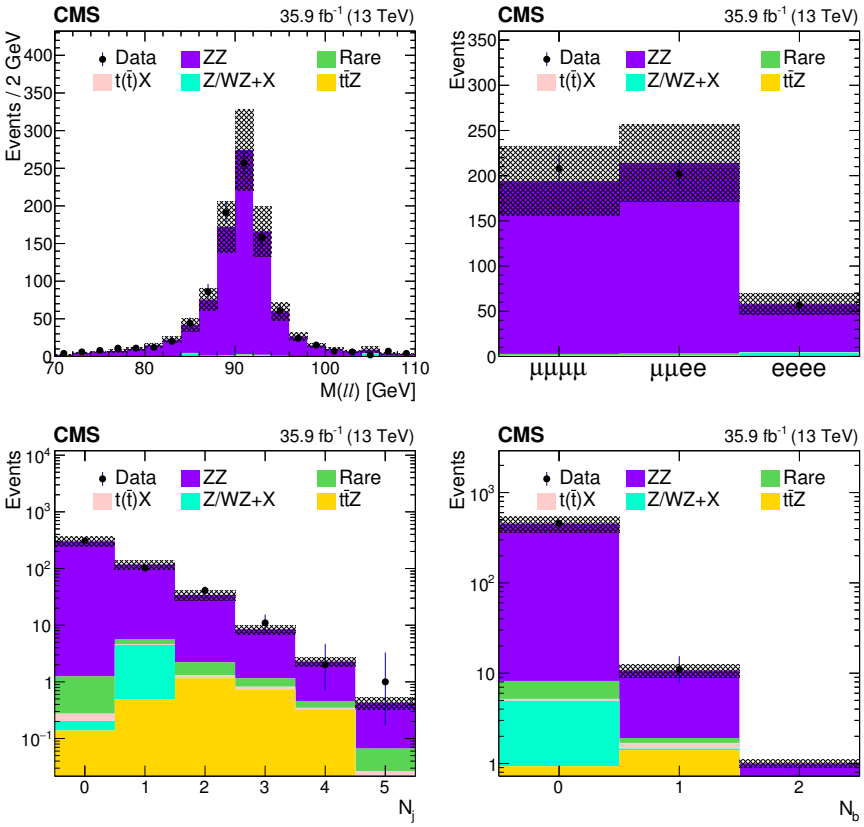

Figure 7. Comparison of data with MC predictions for the mass of the Z boson candidate (upper left), event yields (upper right), jet multiplicity (lower left) and b jet multiplicity (lower right) in a ZZ-dominated background control region. The shaded band represents the total uncertainty in the prediction of the background and the signal processes.

Reconstructed lepton selection efficiencies are measured using a "tag-and-probe" method [43, 44] in bins of lepton p_{T} and η, and are higher than 65 (96)% for electrons (muons). These measurements are performed separately in data and in simulation. The differences between these two measurements are typically around 1–4% per lepton, which corresponds to 3–7% for all leptons in the event. The systematic uncertainties related to this source vary between 2 and 7%.

Uncertainties in the jet energy calibrations are estimated by shifting the energy of jets in the simulation up and down by one standard deviation. Depending on p_{T} and η, the uncertainty in jet energy scale changes by 2–5% [45, 46]. For the signal and backgrounds modelled through simulation, the resulting uncertainty is determined by the observed differences in yields with and without the shift in jet energies. The same technique is used to calculate the uncertainties caused by the jet energy resolution, for which the uncertainty is found to be 1–6%. These uncertainties are also propagated in the $p_{\mathrm{T}}^{\mathrm{miss}}$ variable, and the resulting uncertainty in signal selection is found to be around 1%. The b tagging efficiency in the simulation is corrected using scale factors determined from data [33, 34]. These contribute with an uncertainty of about 2–5% on the predicted yields, which depend on p_{T}, η and jet and b-tag multiplicity.

JHEP08(2018)011

To estimate the theoretical uncertainties due to μ_R and μ_F choices, each of these parameters is varied independently up and down by a factor of 2, ignoring the anti-correlated variations. For the acceptance uncertainties, the envelope of the results is used as an uncertainty in each search bin, and found not to exceed 2%. The different replicas in the NNPDF30 PDF set [20] are used to estimate the corresponding uncertainty in acceptance, which is typically less than 1%.

The theoretical uncertainty in the cross sections for top quark (pair) production in association with a Higgs boson or a vector boson is 11% [1]. For the WZ and ZZ backgrounds, the overall uncertainty in the cross section is 10%, with additional uncertainties at large jet multiplicities. Rare SM processes are assigned a 50% systematic uncertainty. All of the experimental uncertainties described above are evaluated for each process in all analysis categories. A 20% systematic uncertainty is assigned to the charge-misidentified background. The uncertainty in the nonprompt lepton contribution in the SS dilepton and three-lepton analyses is 30%, for which the statistical uncertainty in the observed yields in the sideband region is also taken into account.

The theoretical uncertainties for individual backgrounds as well as the systematic uncertainties for the nonprompt background are uncorrelated, but correlated across the analysis categories. The different sources of experimental uncertainty are correlated across the analysis categories and among the background and signal predictions. The statistical uncertainties from the limited number of events in MC simulation and from the data events in the sideband regions are considered fully uncorrelated.

The impact of different sources of systematic uncertainty is estimated by fixing the nuisance parameter corresponding to each uncertainty one at a time and evaluating the decrease in the total systematic uncertainty. Uncertainties associated with the integrated luminosity, lepton identification, trigger selection efficiencies, nonprompt lepton, and $t(\bar{t})X$ backgrounds have the greatest effect on both the $t\bar{t}W$ and the $t\bar{t}Z$ cross section measurements. The full set of systematic uncertainties is shown in table 1.

7 Results

As described in section 4, the data are analyzed in three exclusive channels according to the number of leptons in the final state: SS dilepton, three- and four-lepton events. Each channel is further categorized according to the number of jets and b-tagged jets. The predicted SM background and signal yields, and the observed data are shown in figures 8 and 9, and in tables 2–5, for each of the above categories, respectively. In general, we find good agreement between the predicted yields and the observed data, except for some excess of events accumulated in the $N_j = 2$, 3 and $N_b > 1$ category of the three-lepton channel. Extensive studies were performed to ensure the robustness of the estimated background yields in this region. No hints of a missing or underestimated background were found; therefore, we attribute this excess to a statistical fluctuation in data. In figures 10 and 11, various kinematic distributions in the predicted and observed yields are presented in $t\bar{t}W$ and $t\bar{t}Z$ signal-enriched regions: SS dileptons with $N_j > 2$ and $N_b > 1$, and three-lepton events with $N_j > 2$ and $N_b > 0$, respectively.

JHEP08(2018)011

Source	Uncertainty from each source (%)	Impact on the measured $t\bar{t}W$ cross section (%)	Impact on the measured $t\bar{t}Z$ cross section (%)
Integrated luminosity	2.5	4	3
Jet energy scale and resolution	2–5	3	3
Trigger	2–4	4–5	5
B tagging	1–5	2–5	4–5
PU modeling	1	1	1
Lepton ID efficiency	2–7	3	6–7
Choice in μ_R and μ_F	1	<1	1
PDF	1	<1	1
Nonprompt background	30	4	<2
WZ cross section	10–20	<1	2
ZZ cross section	20	—	1
Charge misidentification	20	3	—
Rare SM background	50	2	2
$t(\bar{t})X$ background	10–15	4	3
Stat. unc. in nonprompt background	5–50	4	2
Stat. unc. in rare SM backgrounds	20–100	1	<1
Total systematic uncertainty	—	14	12

Table 1. Summary of the sources of uncertainties, their magnitudes, and their effects in the final measurement. The first column indicates the source of the uncertainties, while the second column shows the corresponding input uncertainty on each background source and the signal. The third and fourth columns show the resulting uncertainties in the respective $t\bar{t}W$ and $t\bar{t}Z$ cross sections.

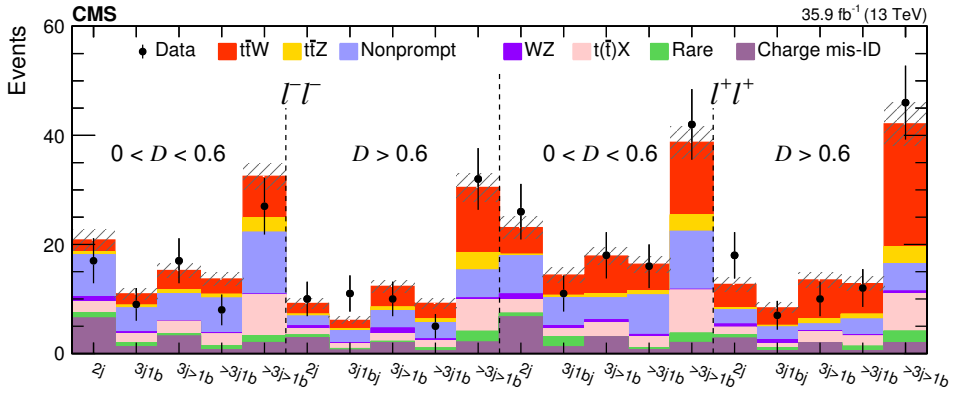

Figure 8. Predicted signal and background yields, as obtained from the fit, compared to observed data in the SS dilepton analysis. The hatched band shows the total uncertainty associated with the signal and background predictions, as obtained from the fit.

The statistical procedure to extract the cross section is detailed in refs. [47–50]. The observed yields and background estimates in each analysis category, described in section 4, and the systematic uncertainties described in section 6 are used to construct a binned likelihood function $L(r, \theta)$ as a product of Poisson probabilities of all bins. The parameter r is the signal-strength modifier and θ represents the full suite of nuisance parameters. The signal strength parameter $r = 1$ corresponds to a signal cross section equal to the SM prediction, while $r = 0$ corresponds to the background-only hypothesis.

The test statistic is the profile likelihood ratio, $q(r) = -2L(r, \hat{\theta}_r)/L(\hat{r}, \hat{\theta})$, and asymptotic approximation is used to extract the fitted cross section, the associated uncertainties,

JHEP08(2018)011

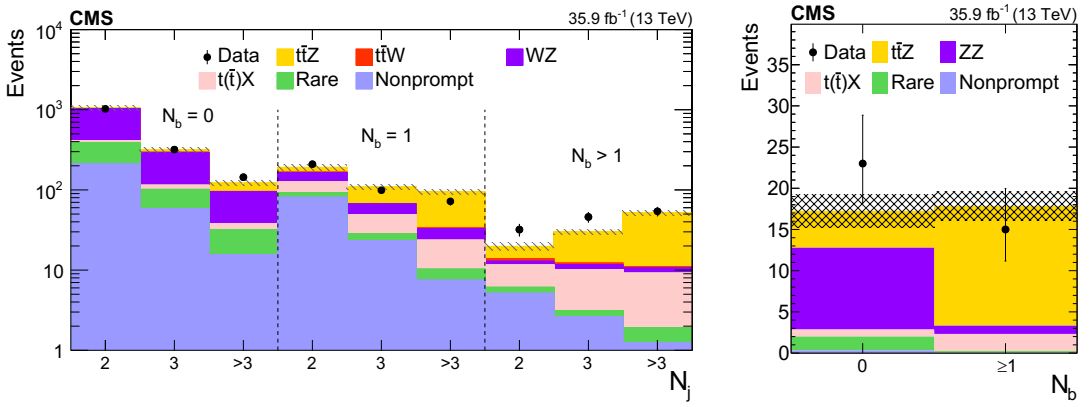

Figure 9. Predicted signal and background yields, as obtained from the fit, compared to observed data in $N_j = 2$, 3, and > 3 categories in the three-lepton analysis (left), and in $N_b = 0$, 1 categories in the four-lepton analysis (right). The hatched band shows the total uncertainty associated with the signal and background predictions, as obtained from the fit.

Process	$N_j = 2$	$N_j = 3$	$N_j > 3$
Nonprompt	136.5 ± 13.9	110.3 ± 11.3	57.3 ± 6.1
Total background	192.1 ± 15.6	137.7 ± 11.7	74.0 ± 6.4
$t\bar{t}W$	13.1 ± 0.3	17.6 ± 0.3	13.8 ± 0.3
$t\bar{t}Z$	1.6 ± 0.4	3.1 ± 0.7	4.4 ± 1.0
Total	206.8 ± 15.7	158.4 ± 11.8	92.3 ± 6.5
Observed	229	144	92

Table 2. Predicted signal and background yields, as obtained from the fit, compared to observed data in the SS dilepton channel for the $D < 0$ region, i.e. the nonprompt lepton control region. The total uncertainty obtained from the fit is also shown.

and the significance of the observation of the signal process [47–50], where $\hat{\theta}_r$ reflects the values of the nuisance parameters that maximize the likelihood function for signal strength r. The quantities $\hat{r}$ and $\hat{\theta}$ are the values that simultaneously maximize L.

The measurement of the individual cross sections for $t\bar{t}W$ and $t\bar{t}Z$ is performed using the events in the SS dilepton, and the three- and four-lepton categories, respectively, while the $t\bar{t}W^+(t\bar{t}W^-)$ signal extraction is performed using the SS dilepton category with $\ell^+\ell^+(\ell^-\ell^-)$. The summary of the expected and observed signal significances for each of these processes is given in table 6. We find an expected (observed) signal significance of 4.5 (5.3) standard deviations in the SS dilepton channel, and 4.7 (4.5) standard deviations in the four-lepton channel, while in three-lepton channel both the expected and the observed significances are found to be much larger than 5 standard deviations. The expected (observed) signal significances for $t\bar{t}W^+$ and $t\bar{t}W^-$ processes are calculated as well, being 4.2 (5.5) and 2.4 (2.3), respectively.

The measured signal strength parameters are found to be $1.23^{+0.19}_{-0.18}\,(\text{stat})^{+0.20}_{-0.18}\,(\text{syst})^{+0.13}_{-0.12}\,(\text{theo})$ for $t\bar{t}W$, and $1.17\ ^{+0.11}_{-0.10}\,(\text{stat})^{+0.14}_{-0.12}\,(\text{syst})^{+0.11}_{-0.12}\,(\text{theo})$ for $t\bar{t}Z$. These parameters are used to multiply the corresponding theoretical cross sections

JHEP08(2018)011

		N_j	N_b	Background	$t\bar{t}W$	$t\bar{t}Z$	Total	Observed
$\ell^-\ell^-$	$0 < D < 0.6$	2	>0	18.1 ± 1.8	2.2 ± 0.4	0.5 ± 0.1	20.8 ± 1.9	17
		3	1	8.3 ± 0.9	2.1 ± 0.4	0.5 ± 0.1	10.9 ± 0.9	9
			>1	10.9 ± 1.1	3.5 ± 0.6	0.8 ± 0.1	15.2 ± 1.3	17
		>3	1	10.1 ± 1.1	2.8 ± 0.5	0.7 ± 0.2	13.7 ± 1.3	8
			>1	22.2 ± 2.0	7.6 ± 1.2	2.7 ± 0.4	32.5 ± 2.4	27
	$D > 0.6$	2	>0	6.8 ± 0.9	2.0 ± 0.3	0.4 ± 0.1	9.2 ± 0.9	10
		3	1	4.1 ± 0.6	1.6 ± 0.3	0.3 ± 0.1	6.1 ± 0.6	11
			>1	7.8 ± 0.9	3.8 ± 0.6	0.7 ± 0.1	12.3 ± 1.1	10
		>3	1	5.6 ± 0.7	2.9 ± 0.5	0.7 ± 0.2	9.2 ± 0.9	5
			>1	15.3 ± 1.5	12.0 ± 1.9	3.2 ± 0.5	30.5 ± 2.5	32
$\ell^+\ell^+$	$0 < D < 0.6$	2	>0	17.9 ± 1.8	4.9 ± 0.8	0.3 ± 0.1	23.1 ± 2.0	26
		3	1	10.2 ± 1.3	3.7 ± 0.6	0.4 ± 0.1	14.4 ± 1.4	11
			>1	10.2 ± 1.2	6.9 ± 1.1	0.8 ± 0.2	17.9 ± 1.6	18
		>3	1	10.7 ± 1.2	4.9 ± 0.8	0.8 ± 0.2	16.4 ± 1.4	16
			>1	22.4 ± 2.0	13.3 ± 2.2	3.0 ± 0.5	38.7 ± 3.0	42
	$D > 0.6$	2	>0	8.0 ± 1.1	4.3 ± 0.7	0.4 ± 0.1	12.7 ± 1.3	18
		3	1	4.8 ± 0.7	3.2 ± 0.5	0.3 ± 0.1	8.4 ± 0.9	7
			>1	5.4 ± 0.7	7.1 ± 1.2	1.0 ± 0.2	13.5 ± 1.4	10
		>3	1	6.3 ± 0.8	5.6 ± 0.9	0.9 ± 0.2	12.8 ± 1.2	12
			>1	16.5 ± 1.5	22.5 ± 3.7	3.1 ± 0.5	42.1 ± 4.0	46

Table 3. Predicted signal and background yields, as obtained from the fit, compared to observed data in the SS dilepton final state. The total uncertainty obtained from the fit is also shown.

N_b	N_j	Background	$t\bar{t}W$	$t\bar{t}Z$	Total	Observed
0	2	1032.8 ± 77.1	0.9 ± 0.1	18.2 ± 3.2	1051.9 ± 77.2	1022
	3	293.5 ± 21.4	0.4 ± 0.1	22.3 ± 3.9	316.3 ± 21.8	318
	>3	95.4 ± 7.4	0.3 ± 0.1	26.1 ± 4.6	121.8 ± 8.7	144
1	2	164.6 ± 17.8	1.9 ± 0.3	24.3 ± 4.3	190.7 ± 18.3	209
	3	66.6 ± 6.7	0.9 ± 0.2	41.2 ± 7.2	108.7 ± 9.8	99
	>3	32.8 ± 3.3	0.8 ± 0.1	61.3 ± 10.8	94.9 ± 11.3	72
>1	2	12.9 ± 2.4	1.0 ± 0.2	5.9 ± 1.0	19.8 ± 2.6	32
	3	11.6 ± 1.7	0.6 ± 0.1	17.9 ± 3.2	30.1 ± 3.6	46
	>3	10.6 ± 1.6	0.4 ± 0.1	41.0 ± 7.2	52.0 ± 7.4	54

Table 4. Predicted signal and background yields, as obtained from the fit, compared to observed data in the three-lepton final state. The total uncertainty obtained from the fit is also shown.

Process	$N_b = 0$	$N_b > 0$
Total background	12.8 ± 2.0	3.3 ± 0.3
$t\bar{t}Z$	4.5 ± 0.6	14.5 ± 1.8
Total	17.2 ± 2.0	17.8 ± 1.8
Observed	23	15

Table 5. Predicted signal and background yields, as obtained from the fit, compared to observed data in the four-lepton final state. The total uncertainty obtained from the fit is also shown.

JHEP08(2018)011

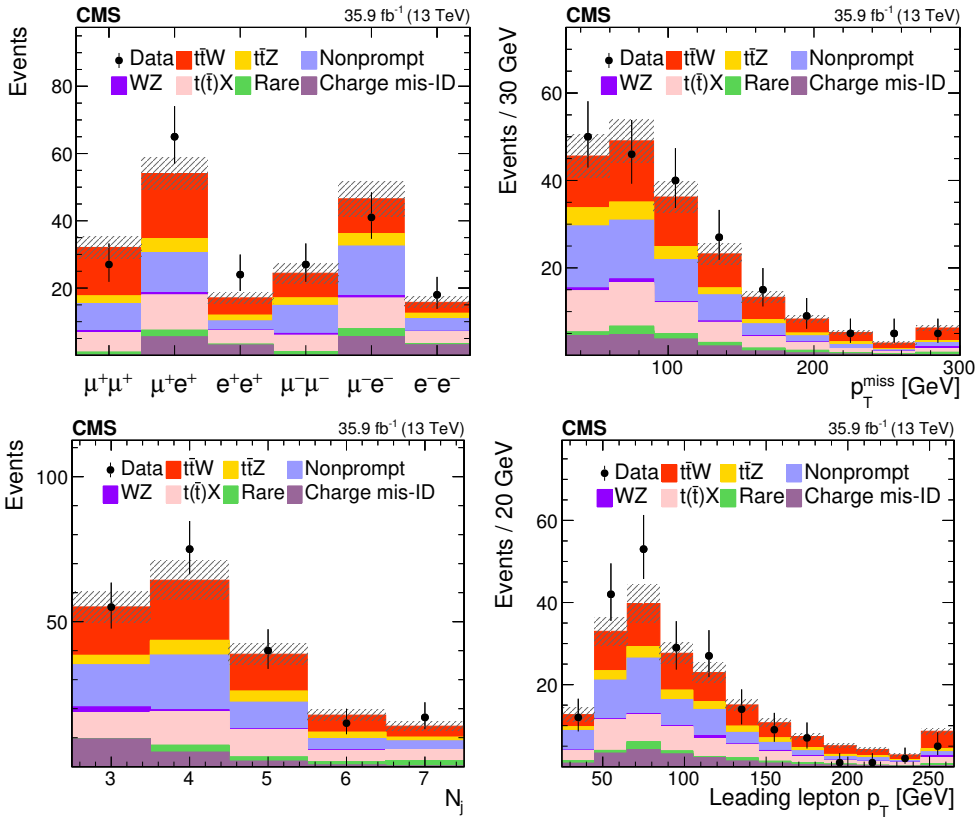

Figure 10. Predicted signal and background yields, as obtained from the fit, compared to observed data versus the flavor and the charge combination of leptons (upper left), $p_{\mathrm{T}}^{\mathrm{miss}}$ (upper right), jet multiplicity (lower left), and the p_{T} of the leading lepton (lower right) in the SS dilepton channel with at least three jets and at least two b jets. The last bin in each distribution includes the overflow events, and the hatched band shows the total uncertainty associated with the signal and background predictions, as obtained from the fit.

Channel	Expected significance	Observed significance
SS dilepton $\ell^-\ell^-$ ($\mathrm{t\bar{t}W^-}$)	2.4	2.3
SS dilepton $\ell^+\ell^+$($\mathrm{t\bar{t}W^+}$)	4.2	5.5
SS dilepton $\ell^\pm\ell^\pm$ ($\mathrm{t\bar{t}W^\pm}$)	4.5	5.3
Three-lepton ($\mathrm{t\bar{t}Z}$)	>5.0	>5.0
Four-lepton ($\mathrm{t\bar{t}Z}$)	4.7	4.5
Three- and four-lepton combined ($\mathrm{t\bar{t}Z}$)	>5.0	>5.0

Table 6. Summary of expected and observed significances (in standard deviations) for $\mathrm{t\bar{t}W}$ and $\mathrm{t\bar{t}Z}$.

for $\mathrm{t\bar{t}W}$ and $\mathrm{t\bar{t}Z}$ mentioned in section 3, to obtain the measured cross sections for $\mathrm{t\bar{t}W}$ and $\mathrm{t\bar{t}Z}$:

$$\sigma(\mathrm{pp} \to \mathrm{t\bar{t}W}) = 0.77^{+0.12}_{-0.11}\,(\mathrm{stat})^{+0.13}_{-0.12}\,(\mathrm{syst})\,\mathrm{pb},$$

$$\sigma(\mathrm{pp} \to \mathrm{t\bar{t}Z}) = 0.99^{+0.09}_{-0.08}\,(\mathrm{stat})^{+0.12}_{-0.10}\,(\mathrm{syst})\,\mathrm{pb}.$$

JHEP08(2018)011

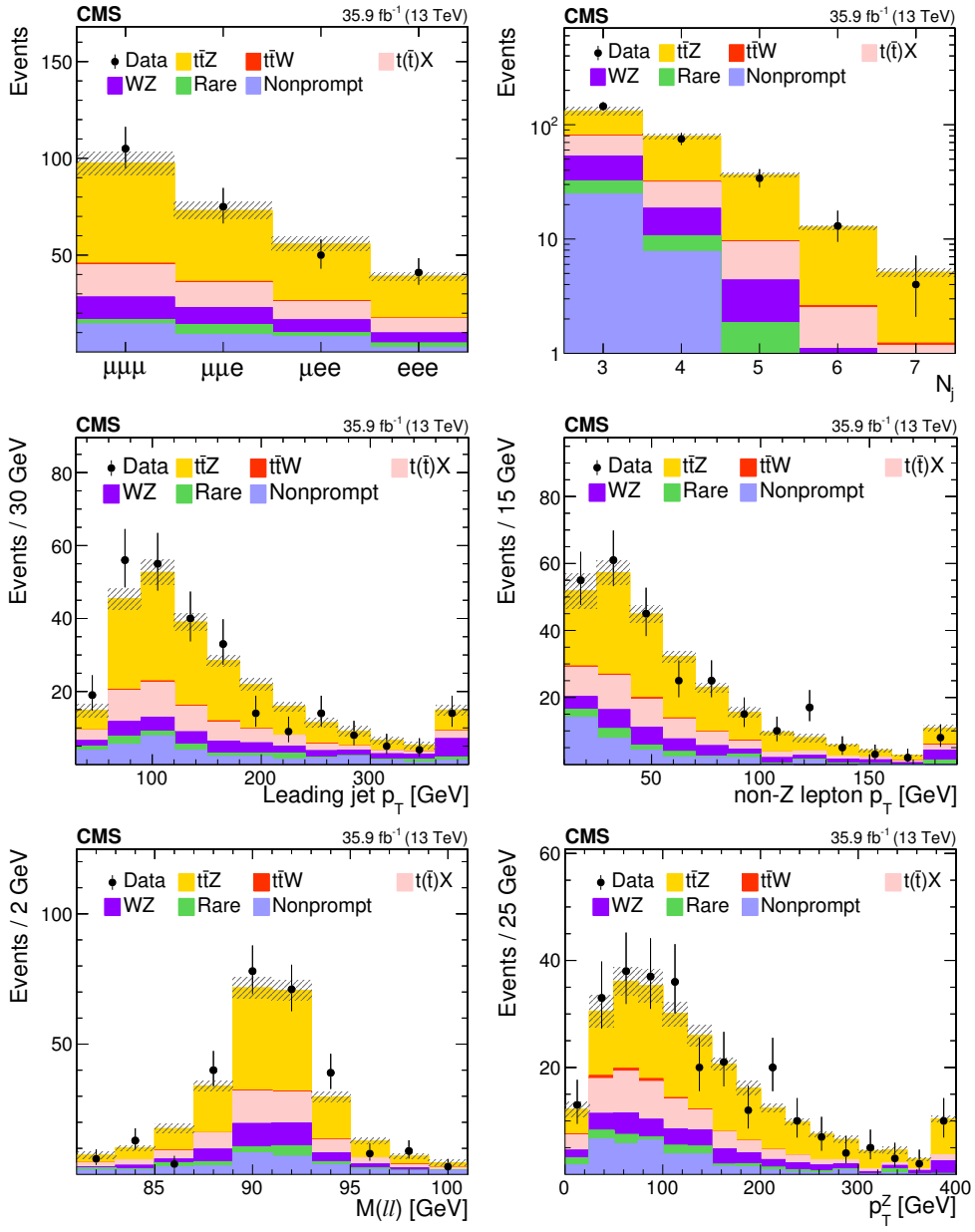

Figure 11. Predicted signal and background yields, as obtained from the fit, compared to observed data in the three-lepton channel for events containing at least three jets and at least one b jet. From left to right: the lepton flavor and jet multiplicity (upper), p_{T} of the leading jet and the lepton not used to form Z (central), and invariant mass of the OSSF lepton pair and p_{T} of the reconstructed Z boson (lower). The last bin in each distribution includes the overflow events, and the hatched band shows the total uncertainty associated with the signal and background predictions, as obtained from the fit.

JHEP08(2018)011

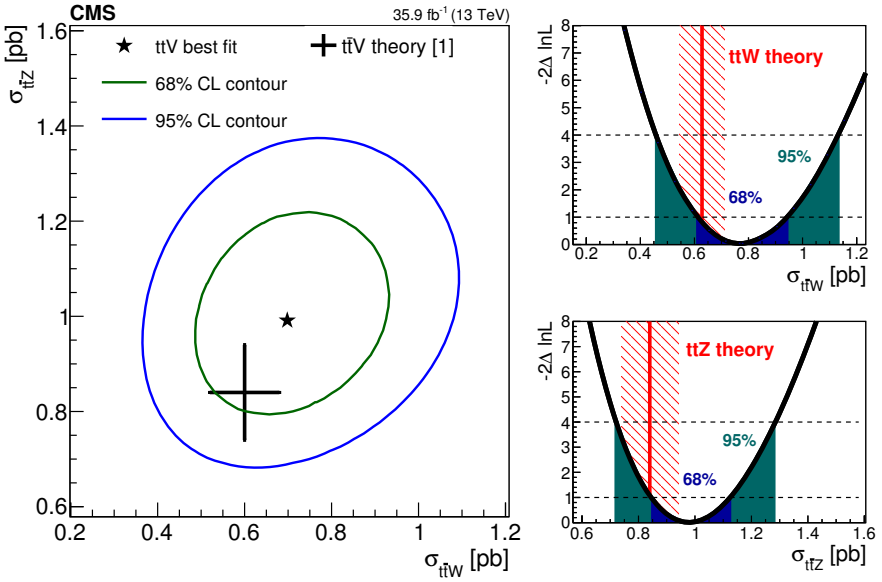

Figure 12. Result of the simultaneous fit for $t\bar{t}W$ and $t\bar{t}Z$ cross sections (denoted as star), along with its 68 and 95% CL contours are shown on the left panel. The right panel presents the individual measured cross sections along with the 68 and 95% CL intervals and the theory prediction [1] with their respective uncertainties for $t\bar{t}W$ and $t\bar{t}Z$.

The measured cross sections for the $t\bar{t}W^+$ and $t\bar{t}W^-$ processes are:

$$\sigma(pp \to t\bar{t}W^+) = 0.58 \pm 0.09\,(\text{stat})^{+0.09}_{-0.08}\,(\text{syst})\,\text{pb},$$

$$\sigma(pp \to t\bar{t}W^-) = 0.19 \pm 0.07\,(\text{stat}) \pm 0.06\,(\text{syst})\,\text{pb}.$$

The individual measured cross sections for $t\bar{t}W$ and $t\bar{t}Z$, as well as the results of a simultaneous fit for these cross sections in all three analysis categories, SS dilepton, three-lepton, and four-lepton, are summarized in figure 12. The corresponding 68 and 95% confidence level (CL) contours and intervals are also shown. The cross section extracted for $t\bar{t}Z$ from the simultaneous fit is identical to the one obtained from the individual measurement, while for $t\bar{t}W$ the simultaneous fit result is shifted down by about 6%, which is smaller than the total systematic uncertainty. This is because the fitted value for the nonprompt background contribution in the three-lepton channel is 9% higher than the nominal value, so the fitted nonprompt yields in the SS dilepton channel are higher in the combined fit compared to the one in the individual fit.

8 Effective field theory interpretation

Within the framework of effective field theory, cross section measurements can be used to search for NP in a model-independent way at energy scales that are not yet experimentally accessible. Using this approach, the SM Lagrangian is extended with higher-order operators that correspond to combinations of SM fields. The extended Lagrangian is a

JHEP08(2018)011

series expansion in the inverse of the energy scale of the NP, $1/\Lambda$ [51], hence operators are suppressed as long as Λ is large compared with the experimentally-accessible energy.

The effective Lagrangian is (ignoring the single dimension-five operator, which violates lepton number conservation [51])

$$\mathcal{L}_{\text{eff}} = \mathcal{L}_{\text{SM}} + \frac{1}{\Lambda^2}\sum_i c_i \mathcal{O}_i + \cdots , \tag{8.1}$$

where $\mathcal{L}_{\text{SM}}$ is the dimension-four SM Lagrangian, $\mathcal{O}_i$ are dimension-six operators, and the ellipsis symbol represents higher-dimension operators. The dimensionless Wilson coefficients c_i parameterize the strength of the NP interaction.

Assuming baryon and lepton number conservation, there are fifty-nine independent dimension-six operators [52]. Thirty-nine of these operators were chosen for study in ref. [53] because they include at least one Higgs field; the four-fermion operators were omitted. Constraints on the Wilson coefficients of some dimension-six operators have been reported in refs. [2, 6, 54–60].

To investigate the effects of NP on any given process, it is necessary to calculate the expected cross section as a function of the Wilson coefficients. The matrix element can be written as the sum of SM and NP components:

$$\mathcal{M} = \mathcal{M}_0 + \sum_i c_i \mathcal{M}_i. \tag{8.2}$$

In this work, we consider one operator at a time. The cross section is proportional to the square of the matrix element, and has the following structure [57]:

$$\begin{aligned} \sigma_{\text{SM+NP}}(c_i) &\propto |\mathcal{M}|^2 \\ &\propto s_0 + s_{1i}c_i + s_{2i}c_i^2. \end{aligned} \tag{8.3}$$

The coupling structures s_0, s_{1i}, and s_{2i} are constants which can be determined by evaluating the cross section for at least three values of c_i. Note that while $\sigma(c_i)$ is always quadratic, the minimum is not constrained to appear at the SM value ($c_i = 0$), and in cases of destructive interference with the SM, it is possible to have $\sigma_{\text{SM+NP}}(c_i) < \sigma_{\text{SM}}$.

NP effects on $t\bar{t}W$ and $t\bar{t}Z$ are considered. Because $t\bar{t}H$ is sizeable background to $t\bar{t}W$, and the NP effects on $t\bar{t}H$ are considered as well, as they cannot be disentangled from NP effects on $t\bar{t}W$. The range of Wilson coefficient values to study is chosen such that $|c_i| < (4\pi)^2$ [61]. The dimension-six operators are encoded using the FeynRules [62] implementation from ref. [53], and we follow their notation and operator-naming scheme throughout this work. This implementation assumes flavor-independent fermion couplings. Because the W and Z boson couplings to light quarks are highly constrained by other measurements, i.e. inclusive W or Z cross section measurements, we removed all NP couplings to the first two generations. This modified implementation is used in MadGraph5_aMC@NLO [63] to evaluate the cross section $\sigma_{\text{SM+NP}}$ expected due to both SM and NP effects at LO, with no constraints on the number of allowed QCD or electroweak vertices, for 30 values of c_i, with all other couplings set to their SM values. We then fit those points with a quadratic function (see eq. (8.3)) to determine $\sigma_{\text{SM+NP}}(c_i)$.

JHEP08(2018)011

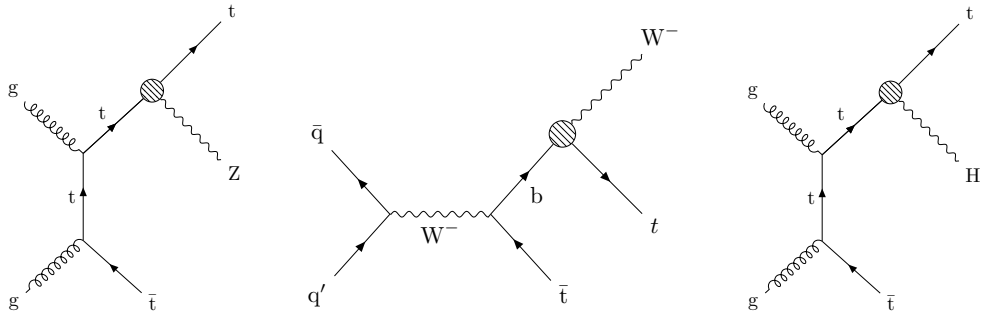

Figure 13. Feynman diagrams representing some of the most significant NP contributions to the $t\bar{t}Z$, $t\bar{t}W$, and $t\bar{t}H$ processes.

The signal strength $r_{t\bar{t}Z}(c_i)$ is defined as the ratio of $\sigma_{\text{SM+NP, }t\bar{t}Z}(c_i)$ to $\sigma_{\text{SM+NP, }t\bar{t}Z}(0)$, and similarly for $t\bar{t}W$ and $t\bar{t}H$. We use this to construct a profile likelihood test statistic $q(c_i)$. The likelihood statistic is maximized to find the asymptotic best fit c_i, similarly to the procedure described in section 7. Each coupling is profiled with the other couplings set to their SM values.

Of the thirty-nine operators in ref. [53], we choose not to consider operators that do not affect $t\bar{t}W$, $t\bar{t}Z$, or $t\bar{t}H$. The expected 95% CL interval is calculated for the remaining 24 operators. We also exclude from consideration operators that produce large effects in better-measured processes for Wilson coefficient values to which our measurement is sensitive. To accomplish this, we require that the cross section for each of $t\bar{t}$, WW, ZZ, WZ, and inclusive Higgs boson production is not modified by more than 70% within our expected 95% CL interval. Finally, we do not include any operators that produce a significant effect on background yields (as described in section 5) other than $t\bar{t}H$, as these can be studied more effectively in other signal regions.

Eight operators satisfy the above requirements, and constraints on their Wilson coefficients, $\bar{c}_{\text{uW}}$, $\bar{c}_{\text{H}}$, $\widetilde{c}_{\text{3G}}$, $\bar{c}_{\text{3G}}$, $\bar{c}_{\text{uG}}$, $\bar{c}_{\text{uB}}$, $\bar{c}_{\text{Hu}}$, and $\bar{c}_{\text{2G}}$ are reported here. Feynman diagrams representing some of the most significant NP contributions to the $t\bar{t}Z$, $t\bar{t}W$, and $t\bar{t}H$ processes are shown in figure 13.

The expected CL intervals for the selected Wilson coefficients are summarized in table 7. Observed best fit values and CL intervals are summarized in table 8. For three representative operators, the calculated signal strengths $r_{t\bar{t}Z}(c_i)$, $r_{t\bar{t}W}(c_i)$, and $r_{t\bar{t}H}(c_i)$ are shown in the left panels of figure 14. The profile likelihood scan is presented in the center panels. In the right panels, results are shown in the $\sigma_{t\bar{t}Z}$ versus $\sigma_{t\bar{t}W}$ plane. The 68% and 95% contours are obtained by sampling randomly from the fitted covariance matrix and extracting the contours which enclose 68.27% and 95.45% of the samples. We remove any assumptions about the energy scale of the NP made in ref. [53] and report the ratio c_i/Λ^2. In cases where $\sigma_{\text{SM+NP}}(c_i)$ has the same minimum for all three processes, the profile likelihood is symmetric around this point, and we present results for $|c_i - c_{i,\text{min}}|$ to make this symmetry explicit.

JHEP08(2018)011

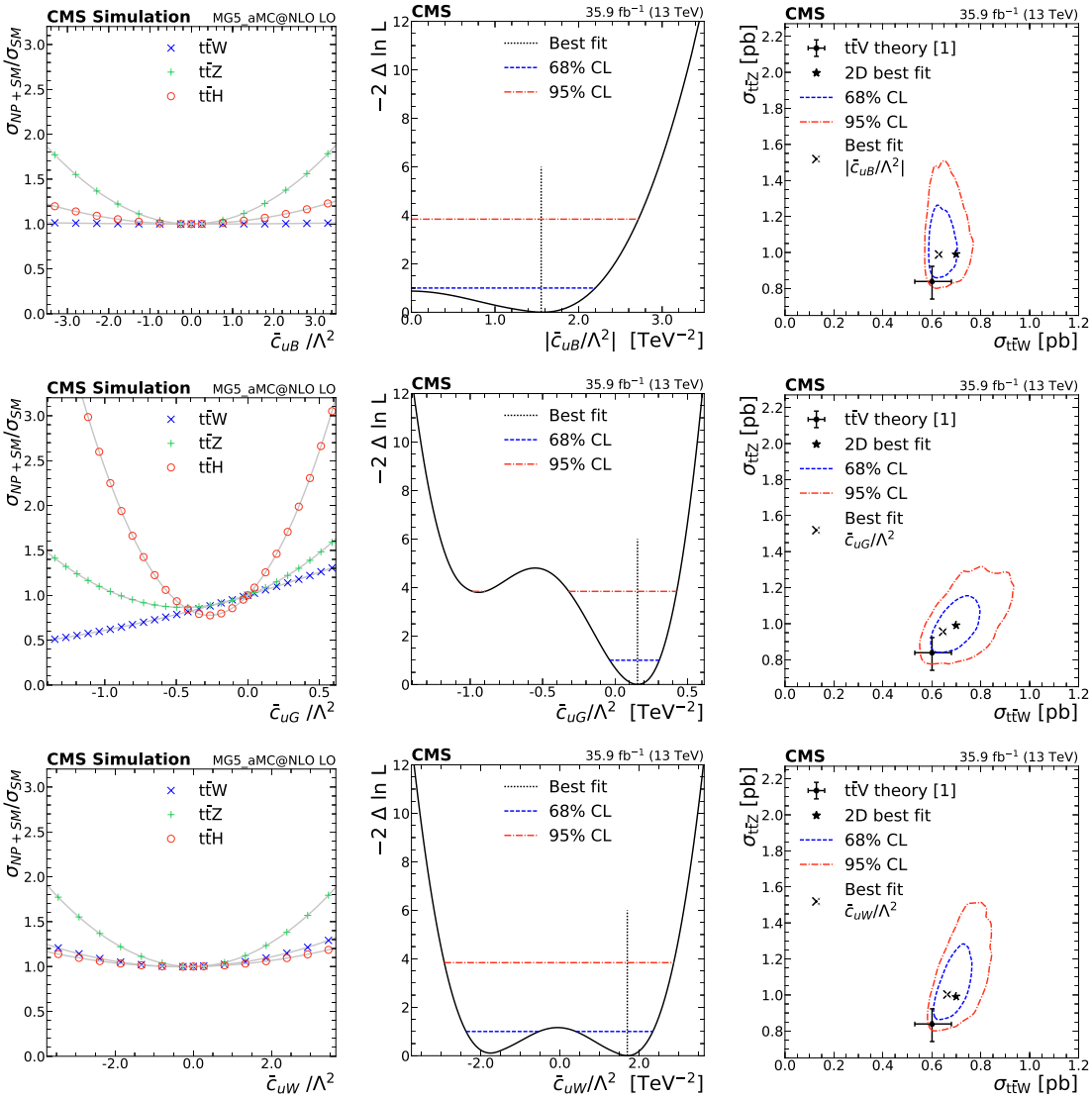

Figure 14. Left: signal strength as a function of selected Wilson coefficients for $t\bar{t}W$ (crosses), $t\bar{t}Z$ (pluses), and $t\bar{t}H$ (circles). Center: the 1D test statistic $q(c_i)$ scan as a function of c_i, profiling all other nuisance parameters. The global best fit value is indicated by a dotted line. Dashed and dash-dotted lines indicate 68% and 95% CL intervals, respectively. Right: the $t\bar{t}Z$ and $t\bar{t}W$ cross section corresponding to the global best fit c_i value is shown as a cross, along with the corresponding 68% (dashed) and 95% (dash-dotted) contours. The two-dimensional best fit to the $t\bar{t}W$ and $t\bar{t}Z$ cross sections is given by the star. The theory predictions [1] for $t\bar{t}W$ and $t\bar{t}Z$ are shown as a dot with bars representing their respective uncertainties.

JHEP08(2018)011

Wilson coefficient	68% CL [TeV^{-2}]	95% CL [TeV^{-2}]
$\bar{c}_{\mathrm{uW}}/\Lambda^2$	$[-1.6, 1.5]$	$[-2.2, 2.2]$
$\lvert\bar{c}_{\mathrm{H}}/\Lambda^2 - 16.8\,\mathrm{TeV}^{-2}\rvert$	$[3.7, 23.4]$	$[0, 28.7]$
$\widetilde{c}_{\mathrm{3G}}/\Lambda^2$	$[-0.5, 0.5]$	$[-0.7, 0.7]$
$\bar{c}_{\mathrm{3G}}/\Lambda^2$	$[-0.3, 0.7]$	$[-0.5, 0.9]$
$\bar{c}_{\mathrm{uG}}/\Lambda^2$	$[-0.9, -0.8]$ and $[-0.3, 0.2]$	$[-1.1, 0.3]$
$\lvert\bar{c}_{\mathrm{uB}}/\Lambda^2\rvert$	$[0, 1.5]$	$[0, 2.1]$
$\bar{c}_{\mathrm{Hu}}/\Lambda^2$	$[-9.2, -6.5]$ and $[-1.6, 1.1]$	$[-10.1, 2.0]$
$\bar{c}_{\mathrm{2G}}/\Lambda^2$	$[-0.7, 0.4]$	$[-0.9, 0.6]$

Table 7. Expected 68% and 95% CL intervals for selected Wilson coefficients.

Wilson coefficient	Best fit [TeV^{-2}]	68% CL [TeV^{-2}]	95% CL [TeV^{-2}]
$\bar{c}_{\mathrm{uW}}/\Lambda^2$	1.7	$[-2.4, -0.5]$ and $[0.4, 2.4]$	$[-2.9, 2.9]$
$\lvert\bar{c}_{\mathrm{H}}/\Lambda^2 - 16.8\ \mathrm{TeV}^{-2}\rvert$	15.6	$[0, 23.0]$	$[0, 28.5]$
$\lvert\widetilde{c}_{\mathrm{3G}}/\Lambda^2\rvert$	0.5	$[0, 0.7]$	$[0, 0.9]$
$\bar{c}_{\mathrm{3G}}/\Lambda^2$	-0.4	$[-0.6, 0.1]$ and $[0.4, 0.7]$	$[-0.7, 1.0]$
$\bar{c}_{\mathrm{uG}}/\Lambda^2$	0.2	$[0, 0.3]$	$[-1.0, -0.9]$ and $[-0.3, 0.4]$
$\lvert\bar{c}_{\mathrm{uB}}/\Lambda^2\rvert$	1.6	$[0, 2.2]$	$[0, 2.7]$
$\bar{c}_{\mathrm{Hu}}/\Lambda^2$	-9.3	$[-10.3, -8.0]$ and $[0, 2.1]$	$[-11.1, -6.5]$ and $[-1.6, 3.0]$
$\bar{c}_{\mathrm{2G}}/\Lambda^2$	0.4	$[-0.9, -0.3]$ and $[-0.1, 0.6]$	$[-1.1, 0.8]$

Table 8. Observed best fit values for selected Wilson coefficients determined from this $\mathrm{t\bar{t}W}$ and $\mathrm{t\bar{t}Z}$ measurement, along with corresponding 68% and 95% CL intervals. In some cases the profile likelihood shows another local minimum that cannot be excluded; the number reported here is the global minimum.

9 Summary

A measurement of top quark pair production in association with a W or a Z boson using proton-proton collisions at 13 TeV is presented. The analysis is performed in the same-sign dilepton final state for $\mathrm{t\bar{t}W}$, and the three- and four-lepton final states for $\mathrm{t\bar{t}Z}$, and these three final states are used to extract the cross sections for $\mathrm{t\bar{t}W}$ and $\mathrm{t\bar{t}Z}$ production. For both processes the observed signal significance exceeds 5 standard deviations. The measured signal strength parameters are $1.23^{+0.19}_{-0.18}\,(\mathrm{stat})^{+0.20}_{-0.18}\,(\mathrm{syst})^{+0.13}_{-0.12}\,(\mathrm{theo})$ and $1.17\ ^{+0.11}_{-0.10}\,(\mathrm{stat})^{+0.14}_{-0.12}\,(\mathrm{syst})^{+0.11}_{-0.12}\,(\mathrm{theo})$ for $\mathrm{t\bar{t}W}$ and $\mathrm{t\bar{t}Z}$, respectively. The measured cross sections are $\sigma(\mathrm{t\bar{t}W}) = 0.77^{+0.12}_{-0.11}\,(\mathrm{stat})^{+0.13}_{-0.12}\,(\mathrm{syst})\,\mathrm{pb}$ and $\sigma(\mathrm{t\bar{t}Z}) = 0.99^{+0.09}_{-0.08}\,(\mathrm{stat})^{+0.12}_{-0.10}\,(\mathrm{syst})\,\mathrm{pb}$, in agreement with the standard model predictions. These results have been used to set constraints on the Wilson coefficients of dimension-six operators. Eight operators have been identified which are of particular interest because they change the expected cross sections of $\mathrm{t\bar{t}Z}$, $\mathrm{t\bar{t}W}$, or $\mathrm{t\bar{t}H}$ without significantly impacting expected background yields. Both $\mathrm{t\bar{t}Z}$ and $\mathrm{t\bar{t}H}$ are affected by $\mathcal{O}_{\mathrm{3G}}$, $\mathcal{O}_{\widetilde{\mathrm{3G}}}$, $\mathcal{O}_{\mathrm{2G}}$, and $\mathcal{O}_{\mathrm{uB}}$. Only $\mathrm{t\bar{t}Z}$ is affected by $\mathcal{O}_{\mathrm{Hu}}$, while $\mathcal{O}_{\mathrm{H}}$ affects only $\mathrm{t\bar{t}H}$. All three processes $\mathrm{t\bar{t}Z}$, $\mathrm{t\bar{t}W}$, and $\mathrm{t\bar{t}H}$ are affected by $\mathcal{O}_{\mathrm{uG}}$ and $\mathcal{O}_{\mathrm{uW}}$. In cases where new physics beyond the standard model modifies the expected $\mathrm{t\bar{t}Z}$ cross section, the sensitivity is mainly determined by $\mathrm{t\bar{t}Z}$ and the fit is able to match the observed excess in data. No operators were identified which provide an independent handle on $\mathrm{t\bar{t}W}$. The constraints presented, obtained by considering one operator at a time, are a useful first step toward more global approaches.

JHEP08(2018)011

Acknowledgments

We congratulate our colleagues in the CERN accelerator departments for the excellent performance of the LHC and thank the technical and administrative staffs at CERN and at other CMS institutes for their contributions to the success of the CMS effort. In addition, we gratefully acknowledge the computing centers and personnel of the Worldwide LHC Computing Grid for delivering so effectively the computing infrastructure essential to our analyses. Finally, we acknowledge the enduring support for the construction and operation of the LHC and the CMS detector provided by the following funding agencies: BMWFW and FWF (Austria); FNRS and FWO (Belgium); CNPq, CAPES, FAPERJ, and FAPESP (Brazil); MES (Bulgaria); CERN; CAS, MoST, and NSFC (China); COLCIENCIAS (Colombia); MSES and CSF (Croatia); RPF (Cyprus); SENESCYT (Ecuador); MoER, ERC IUT, and ERDF (Estonia); Academy of Finland, MEC, and HIP (Finland); CEA and CNRS/IN2P3 (France); BMBF, DFG, and HGF (Germany); GSRT (Greece); OTKA and NIH (Hungary); DAE and DST (India); IPM (Iran); SFI (Ireland); INFN (Italy); MSIP and NRF (Republic of Korea); LAS (Lithuania); MOE and UM (Malaysia); BUAP, CINVESTAV, CONACYT, LNS, SEP, and UASLP-FAI (Mexico); MBIE (New Zealand); PAEC (Pakistan); MSHE and NSC (Poland); FCT (Portugal); JINR (Dubna); MON, RosAtom, RAS, RFBR and RAEP (Russia); MESTD (Serbia); SEIDI, CPAN, PCTI and FEDER (Spain); Swiss Funding Agencies (Switzerland); MST (Taipei); ThEPCenter, IPST, STAR, and NSTDA (Thailand); TUBITAK and TAEK (Turkey); NASU and SFFR (Ukraine); STFC (United Kingdom); DOE and NSF (U.S.A.).

Individuals have received support from the Marie-Curie program and the European Research Council and Horizon 2020 Grant, contract No. 675440 (European Union); the Leventis Foundation; the A. P. Sloan Foundation; the Alexander von Humboldt Foundation; the Belgian Federal Science Policy Office; the Fonds pour la Formation à la Recherche dans l'Industrie et dans l'Agriculture (FRIA-Belgium); the Agentschap voor Innovatie door Wetenschap en Technologie (IWT-Belgium); the Ministry of Education, Youth and Sports (MEYS) of the Czech Republic; the Council of Science and Industrial Research, India; the HOMING PLUS program of the Foundation for Polish Science, cofinanced from European Union, Regional Development Fund, the Mobility Plus program of the Ministry of Science and Higher Education, the National Science Center (Poland), contracts Harmonia 2014/14/M/ST2/00428, Opus 2014/13/B/ST2/02543, 2014/15/B/ST2/03998, and 2015/19/B/ST2/02861, Sonata-bis 2012/07/E/ST2/01406; the National Priorities Research Program by Qatar National Research Fund; the Programa Severo Ochoa del Principado de Asturias; the Thalis and Aristeia programs cofinanced by EU-ESF and the Greek NSRF; the Rachadapisek Sompot Fund for Postdoctoral Fellowship, Chulalongkorn University and the Chulalongkorn Academic into Its 2nd Century Project Advancement Project (Thailand); the Welch Foundation, contract C-1845; and the Weston Havens Foundation (U.S.A.).

JHEP08(2018)011

References

[1] LHC Higgs Cross Section Working Group collaboration, D. de Florian et al., *Handbook of LHC Higgs cross sections: 4. Deciphering the nature of the Higgs sector*, arXiv:1610.07922 [INSPIRE].

[2] O. Bessidskaia Bylund et al., *Probing top quark neutral couplings in the standard model effective field theory at NLO in QCD*, *JHEP* **05** (2016) 052 [arXiv:1601.08193] [INSPIRE].

[3] C. Englert, R. Kogler, H. Schulz and M. Spannowsky, *Higgs coupling measurements at the LHC*, *Eur. Phys. J.* **C 76** (2016) 393 [arXiv:1511.05170] [INSPIRE].

[4] CMS collaboration, *Measurement of associated production of vector bosons and top quark-antiquark pairs at* $\sqrt{s} = 7$ *TeV*, *Phys. Rev. Lett.* **110** (2013) 172002 [arXiv:1303.3239] [INSPIRE].

[5] CMS collaboration, *Measurement of top quark-antiquark pair production in association with a W or Z boson in pp collisions at* $\sqrt{s} = 8$ *TeV*, *Eur. Phys. J.* **C 74** (2014) 3060 [arXiv:1406.7830] [INSPIRE].

[6] CMS collaboration, *Observation of top quark pairs produced in association with a vector boson in pp collisions at* $\sqrt{s} = 8$ *TeV*, *JHEP* **01** (2016) 096 [arXiv:1510.01131] [INSPIRE].

[7] ATLAS collaboration, *Measurement of the* $t\bar{t}W$ *and* $t\bar{t}Z$ *production cross sections in pp collisions at* $\sqrt{s} = 8$ *TeV with the ATLAS detector*, *JHEP* **11** (2015) 172 [arXiv:1509.05276] [INSPIRE].

[8] ATLAS collaboration, *Measurement of the* $t\bar{t}Z$ *and* $t\bar{t}W$ *production cross sections in multilepton final states using* $3.2\,fb^{-1}$ *of pp collisions at* $\sqrt{s} = 13$ *TeV with the ATLAS detector*, *Eur. Phys. J.* **C 77** (2017) 40 [arXiv:1609.01599] [INSPIRE].

[9] K.G. Wilson, *Nonlagrangian models of current algebra*, *Phys. Rev.* **179** (1969) 1499 [INSPIRE].

[10] CMS collaboration, *The CMS experiment at the CERN LHC*, 2008 *JINST* **3** S08004 [INSPIRE].

[11] CMS collaboration, *The CMS trigger system*, 2017 *JINST* **12** P01020 [arXiv:1609.02366] [INSPIRE].

[12] J. Alwall et al., *The automated computation of tree-level and next-to-leading order differential cross sections and their matching to parton shower simulations*, *JHEP* **07** (2014) 079 [arXiv:1405.0301] [INSPIRE].

[13] S. Alioli, P. Nason, C. Oleari and E. Re, *A general framework for implementing NLO calculations in shower Monte Carlo programs: the POWHEG BOX*, *JHEP* **06** (2010) 043 [arXiv:1002.2581] [INSPIRE].

[14] H.B. Hartanto, B. Jager, L. Reina and D. Wackeroth, *Higgs boson production in association with top quarks in the POWHEG BOX*, *Phys. Rev.* **D 91** (2015) 094003 [arXiv:1501.04498] [INSPIRE].

[15] T. Melia, P. Nason, R. Rontsch and G. Zanderighi, W^+W^-, *WZ and ZZ production in the POWHEG BOX*, *JHEP* **11** (2011) 078 [arXiv:1107.5051] [INSPIRE].

[16] P. Nason and G. Zanderighi, W^+W^- , *WZ and ZZ production in the POWHEG-BOX-V2*, *Eur. Phys. J.* **C 74** (2014) 2702 [arXiv:1311.1365] [INSPIRE].

JHEP08(2018)011

[17] J.M. Campbell and R.K. Ellis, *MCFM for the Tevatron and the LHC*, *Nucl. Phys. Proc. Suppl.* **205-206** (2010) 10 [arXiv:1007.3492] [INSPIRE].

[18] F. Cascioli et al., *ZZ production at hadron colliders in NNLO QCD*, *Phys. Lett.* **B 735** (2014) 311 [arXiv:1405.2219] [INSPIRE].

[19] F. Caola, K. Melnikov, R. Rötsch and L. Tancredi, *QCD corrections to ZZ production in gluon fusion at the LHC*, *Phys. Rev.* **D 92** (2015) 094028 [arXiv:1509.06734] [INSPIRE].

[20] NNPDF collaboration, R.D. Ball et al., *Parton distributions for the LHC Run II*, *JHEP* **04** (2015) 040 [arXiv:1410.8849] [INSPIRE].

[21] T. Sjöstrand, S. Mrenna and P.Z. Skands, *A brief introduction to PYTHIA 8.1*, *Comput. Phys. Commun.* **178** (2008) 852 [arXiv:0710.3820] [INSPIRE].

[22] T. Sjöstrand et al., *An introduction to PYTHIA 8.2*, *Comput. Phys. Commun.* **191** (2015) 159 [arXiv:1410.3012] [INSPIRE].

[23] P. Skands, S. Carrazza and J. Rojo, *Tuning PYTHIA 8.1: the Monash 2013 Tune*, *Eur. Phys. J.* **C 74** (2014) 3024 [arXiv:1404.5630] [INSPIRE].

[24] CMS collaboration, *Event generator tunes obtained from underlying event and multiparton scattering measurements*, *Eur. Phys. J.* **C 76** (2016) 155 [arXiv:1512.00815] [INSPIRE].

[25] J. Alwall et al., *Comparative study of various algorithms for the merging of parton showers and matrix elements in hadronic collisions*, *Eur. Phys. J.* **C 53** (2008) 473 [arXiv:0706.2569] [INSPIRE].

[26] R. Frederix and S. Frixione, *Merging meets matching in MC@NLO*, *JHEP* **12** (2012) 061 [arXiv:1209.6215] [INSPIRE].

[27] GEANT4 collaboration, S. Agostinelli et al., *GEANT4 — a simulation toolkit*, *Nucl. Instrum. Meth.* **A 506** (2003) 250 [INSPIRE].

[28] CMS collaboration, *Particle-flow reconstruction and global event description with the CMS detector*, 2017 *JINST* **12** P10003 [arXiv:1706.04965] [INSPIRE].

[29] M. Cacciari, G.P. Salam and G. Soyez, *The Anti-k(t) jet clustering algorithm*, *JHEP* **04** (2008) 063 [arXiv:0802.1189] [INSPIRE].

[30] M. Cacciari, G.P. Salam and G. Soyez, *FastJet user manual*, *Eur. Phys. J.* **C 72** (2012) 1896 [arXiv:1111.6097] [INSPIRE].

[31] M. Cacciari and G.P. Salam, *Dispelling the N^3 myth for the k_t jet-finder*, *Phys. Lett.* **B 641** (2006) 57 [hep-ph/0512210] [INSPIRE].

[32] CMS collaboration, *Pileup removal algorithms*, CMS-PAS-JME-14-001 (2014).

[33] CMS collaboration, *Identification of b-quark jets with the CMS experiment*, 2013 *JINST* **8** P04013 [arXiv:1211.4462] [INSPIRE].

[34] CMS collaboration, *Identification of b quark jets at the CMS experiment in the LHC Run 2*, CMS-PAS-BTV-15-001 (2015).

[35] PARTICLE DATA GROUP collaboration, C. Patrignani et al., *Review of particle physics*, *Chin. Phys.* **C 40** (2016) 100001 [INSPIRE].

[36] A. Hocker et al., *TMVA, the toolkit for multivariate data analysis with ROOT*, PoS(ACAT)040 [physics/0703039] [INSPIRE].

JHEP08(2018)011

[37] CMS collaboration, *Search for new physics in same-sign dilepton events in proton-proton collisions at* $\sqrt{s} = 13$ *TeV*, *Eur. Phys. J.* **C 76** (2016) 439 [arXiv:1605.03171] [INSPIRE].

[38] CMS collaboration, *Search for physics beyond the standard model in events with two leptons of same sign, missing transverse momentum and jets in proton-proton collisions at* $\sqrt{s} = 13$ *TeV*, *Eur. Phys. J.* **C 77** (2017) 578 [arXiv:1704.07323] [INSPIRE].

[39] J. Campbell, R.K. Ellis and R. Röntsch, *Single top production in association with a Z boson at the LHC*, *Phys. Rev.* **D 87** (2013) 114006 [arXiv:1302.3856] [INSPIRE].

[40] S. Frixione, V. Hirschi, D. Pagani, H.S. Shao and M. Zaro, *Electroweak and QCD corrections to top-pair hadroproduction in association with heavy bosons*, *JHEP* **06** (2015) 184 [arXiv:1504.03446] [INSPIRE].

[41] CMS collaboration, *CMS luminosity measurements for the 2016 data taking period*, CMS-PAS-LUM-17-001 (2017).

[42] ATLAS collaboration, *Measurement of the inelastic proton-proton cross section at* $\sqrt{s} = 13$ *TeV with the ATLAS Detector at the LHC*, *Phys. Rev. Lett.* **117** (2016) 182002 [arXiv:1606.02625] [INSPIRE].

[43] CMS collaboration, *Performance of CMS muon reconstruction in pp collision events at* $\sqrt{s} = 7$ *TeV*, 2012 *JINST* **7** P10002 [arXiv:1206.4071] [INSPIRE].

[44] CMS collaboration, *Performance of electron reconstruction and selection with the CMS detector in proton-proton collisions at* $\sqrt{s} = 8$ *TeV*, 2015 *JINST* **10** P06005 [arXiv:1502.02701] [INSPIRE].

[45] CMS collaboration, *Performance of the CMS missing transverse momentum reconstruction in pp data at* $\sqrt{s} = 8$ *TeV*, 2015 *JINST* **10** P02006 [arXiv:1411.0511] [INSPIRE].

[46] CMS collaboration, *Performance of missing energy reconstruction in 13 TeV pp collision data using the CMS detector*, CMS-PAS-JME-16-004 (2016).

[47] T. Junk, *Confidence level computation for combining searches with small statistics*, *Nucl. Instrum. Meth.* **A 434** (1999) 435 [hep-ex/9902006] [INSPIRE].

[48] A.L. Read, *Presentation of search results: the CL(s) technique*, *J. Phys.* **G 28** (2002) 2693 [INSPIRE].

[49] ATLAS and CMS collaborations and The LHC Higgs Combination Group, *Procedure for the LHC Higgs boson search combination in Summer 2011*, ATL-PHYS-PUB-2011-011 (2011).

[50] G. Cowan, K. Cranmer, E. Gross and O. Vitells, *Asymptotic formulae for likelihood-based tests of new physics*, *Eur. Phys. J.* **C 71** (2011) 1554 [*Erratum ibid.* **C 73** (2013) 2501] [arXiv:1007.1727] [INSPIRE].

[51] W. Buchmüller and D. Wyler, *Effective Lagrangian analysis of new interactions and flavor conservation*, *Nucl. Phys.* **B 268** (1986) 621 [INSPIRE].

[52] B. Grzadkowski, M. Iskrzynski, M. Misiak and J. Rosiek, *Dimension-six terms in the standard model lagrangian*, *JHEP* **10** (2010) 085 [arXiv:1008.4884] [INSPIRE].

[53] A. Alloul, B. Fuks and V. Sanz, *Phenomenology of the Higgs effective Lagrangian via FEYNRULES*, *JHEP* **04** (2014) 110 [arXiv:1310.5150] [INSPIRE].

[54] J. Ellis, V. Sanz and T. You, *Complete Higgs sector constraints on dimension-6 operators*, *JHEP* **07** (2014) 036 [arXiv:1404.3667] [INSPIRE].

JHEP08(2018)011

[55] K. Whisnant, J.-M. Yang, B.-L. Young and X. Zhang, *Dimension-six CP conserving operators of the third family quarks and their effects on collider observables*, *Phys. Rev.* **D 56** (1997) 467 [hep-ph/9702305] [INSPIRE].

[56] E.L. Berger, Q.-H. Cao and I. Low, *Model independent constraints among the Wtb, $Zb\bar{b}$ and $Zt\bar{t}$ couplings*, *Phys. Rev.* **D 80** (2009) 074020 [arXiv:0907.2191] [INSPIRE].

[57] R. Röntsch and M. Schulze, *Constraining couplings of top quarks to the Z boson in $t\bar{t}$ + Z production at the LHC*, *JHEP* **07** (2014) 091 [*Erratum ibid.* **09** (2015) 132] [arXiv:1404.1005] [INSPIRE].

[58] E. Malkawi and C.P. Yuan, *A global analysis of the top quark couplings to gauge bosons*, *Phys. Rev.* **D 50** (1994) 4462 [hep-ph/9405322] [INSPIRE].

[59] C. Zhang, N. Greiner and S. Willenbrock, *Constraints on non-standard top quark couplings*, *Phys. Rev.* **D 86** (2012) 014024 [arXiv:1201.6670] [INSPIRE].

[60] A. Tonero and R. Rosenfeld, *Dipole-induced anomalous top quark couplings at the LHC*, *Phys. Rev.* **D 90** (2014) 017701 [arXiv:1404.2581] [INSPIRE].

[61] C. Degrande et al., *Effective field theory: a modern approach to anomalous couplings*, *Annals Phys.* **335** (2013) 21 [arXiv:1205.4231] [INSPIRE].

[62] A. Alloul et al., *FeynRules 2.0 — A complete toolbox for tree-level phenomenology*, *Comput. Phys. Commun.* **185** (2014) 2250 [arXiv:1310.1921] [INSPIRE].

[63] S. Frixione and B.R. Webber, *Matching NLO QCD computations and parton shower simulations*, *JHEP* **06** (2002) 029 [hep-ph/0204244] [INSPIRE].

[64] J. Ellis, *TikZ-Feynman: Feynman diagrams with TikZ*, *Comput. Phys. Commun.* **210** (2017) 103 [arXiv:1601.05437] [INSPIRE].

JHEP08(2018)011

The CMS collaboration

Yerevan Physics Institute, Yerevan, Armenia

A.M. Sirunyan, A. Tumasyan

Institut für Hochenergiephysik, Wien, Austria

W. Adam, F. Ambrogi, E. Asilar, T. Bergauer, J. Brandstetter, E. Brondolin, M. Dragicevic, J. Erö, A. Escalante Del Valle, M. Flechl, M. Friedl, R. Frühwirth[1], V.M. Ghete, J. Grossmann, J. Hrubec, M. Jeitler[1], A. König, N. Krammer, I. Krätschmer, D. Liko, T. Madlener, I. Mikulec, E. Pree, N. Rad, H. Rohringer, J. Schieck[1], R. Schöfbeck, M. Spanring, D. Spitzbart, W. Waltenberger, J. Wittmann, C.-E. Wulz[1], M. Zarucki

Institute for Nuclear Problems, Minsk, Belarus

V. Chekhovsky, V. Mossolov, J. Suarez Gonzalez

Universiteit Antwerpen, Antwerpen, Belgium

E.A. De Wolf, D. Di Croce, X. Janssen, J. Lauwers, M. Van De Klundert, H. Van Haevermaet, P. Van Mechelen, N. Van Remortel

Vrije Universiteit Brussel, Brussel, Belgium

S. Abu Zeid, F. Blekman, J. D'Hondt, I. De Bruyn, J. De Clercq, K. Deroover, G. Flouris, D. Lontkovskyi, S. Lowette, I. Marchesini, S. Moortgat, L. Moreels, Q. Python, K. Skovpen, S. Tavernier, W. Van Doninck, P. Van Mulders, I. Van Parijs

Université Libre de Bruxelles, Bruxelles, Belgium

D. Beghin, B. Bilin, H. Brun, B. Clerbaux, G. De Lentdecker, H. Delannoy, B. Dorney, G. Fasanella, L. Favart, R. Goldouzian, A. Grebenyuk, A.K. Kalsi, T. Lenzi, J. Luetic, T. Maerschalk, A. Marinov, T. Seva, E. Starling, C. Vander Velde, P. Vanlaer, D. Vannerom, R. Yonamine, F. Zenoni

Ghent University, Ghent, Belgium

T. Cornelis, D. Dobur, A. Fagot, M. Gul, I. Khvastunov[2], D. Poyraz, C. Roskas, S. Salva, M. Tytgat, W. Verbeke, N. Zaganidis

Université Catholique de Louvain, Louvain-la-Neuve, Belgium

H. Bakhshiansohi, O. Bondu, S. Brochet, G. Bruno, C. Caputo, A. Caudron, P. David, S. De Visscher, C. Delaere, M. Delcourt, B. Francois, A. Giammanco, M. Komm, G. Krintiras, V. Lemaitre, A. Magitteri, A. Mertens, M. Musich, K. Piotrzkowski, L. Quertenmont, A. Saggio, M. Vidal Marono, S. Wertz, J. Zobec

Centro Brasileiro de Pesquisas Fisicas, Rio de Janeiro, Brazil

W.L. Aldá Júnior, F.L. Alves, G.A. Alves, L. Brito, M. Correa Martins Junior, C. Hensel, A. Moraes, M.E. Pol, P. Rebello Teles

Universidade do Estado do Rio de Janeiro, Rio de Janeiro, Brazil

E. Belchior Batista Das Chagas, W. Carvalho, J. Chinellato[3], E. Coelho, E.M. Da Costa, G.G. Da Silveira[4], D. De Jesus Damiao, S. Fonseca De Souza, L.M. Huertas Guativa, H. Malbouisson, M. Melo De Almeida, C. Mora Herrera, L. Mundim, H. Nogima,

JHEP08(2018)011

L.J. Sanchez Rosas, A. Santoro, A. Sznajder, M. Thiel, E.J. Tonelli Manganote[3], F. Torres Da Silva De Araujo, A. Vilela Pereira

Universidade Estadual Paulista[a], Universidade Federal do ABC[b], São Paulo, Brazil

S. Ahuja[a], C.A. Bernardes[a], T.R. Fernandez Perez Tomei[a], E.M. Gregores[b], P.G. Mercadante[b], S.F. Novaes[a], Sandra S. Padula[a], D. Romero Abad[b], J.C. Ruiz Vargas[a]

Institute for Nuclear Research and Nuclear Energy, Bulgarian Academy of Sciences, Sofia, Bulgaria

A. Aleksandrov, R. Hadjiiska, P. Iaydjiev, M. Misheva, M. Rodozov, M. Shopova, G. Sultanov

University of Sofia, Sofia, Bulgaria

A. Dimitrov, L. Litov, B. Pavlov, P. Petkov

Beihang University, Beijing, China

W. Fang[5], X. Gao[5], L. Yuan

Institute of High Energy Physics, Beijing, China

M. Ahmad, J.G. Bian, G.M. Chen, H.S. Chen, M. Chen, Y. Chen, C.H. Jiang, D. Leggat, H. Liao, Z. Liu, F. Romeo, S.M. Shaheen, A. Spiezia, J. Tao, C. Wang, Z. Wang, E. Yazgan, H. Zhang, S. Zhang, J. Zhao

State Key Laboratory of Nuclear Physics and Technology, Peking University, Beijing, China

Y. Ban, G. Chen, J. Li, Q. Li, S. Liu, Y. Mao, S.J. Qian, D. Wang, Z. Xu, F. Zhang[5]

Tsinghua University, Beijing, China

Y. Wang

Universidad de Los Andes, Bogota, Colombia

C. Avila, A. Cabrera, L.F. Chaparro Sierra, C. Florez, C.F. González Hernández, J.D. Ruiz Alvarez, M.A. Segura Delgado

University of Split, Faculty of Electrical Engineering, Mechanical Engineering and Naval Architecture, Split, Croatia

B. Courbon, N. Godinovic, D. Lelas, I. Puljak, P.M. Ribeiro Cipriano, T. Sculac

University of Split, Faculty of Science, Split, Croatia

Z. Antunovic, M. Kovac

Institute Rudjer Boskovic, Zagreb, Croatia

V. Brigljevic, D. Ferencek, K. Kadija, B. Mesic, A. Starodumov[6], T. Susa

University of Cyprus, Nicosia, Cyprus

M.W. Ather, A. Attikis, G. Mavromanolakis, J. Mousa, C. Nicolaou, F. Ptochos, P.A. Razis, H. Rykaczewski

Charles University, Prague, Czech Republic

M. Finger[7], M. Finger Jr.[7]

JHEP08(2018)011

Universidad San Francisco de Quito, Quito, Ecuador
E. Carrera Jarrin

Academy of Scientific Research and Technology of the Arab Republic of Egypt, Egyptian Network of High Energy Physics, Cairo, Egypt
E. El-khateeb[8], S. Elgammal[9], A. Mohamed[10]

National Institute of Chemical Physics and Biophysics, Tallinn, Estonia
R.K. Dewanjee, M. Kadastik, L. Perrini, M. Raidal, A. Tiko, C. Veelken

Department of Physics, University of Helsinki, Helsinki, Finland
P. Eerola, H. Kirschenmann, J. Pekkanen, M. Voutilainen

Helsinki Institute of Physics, Helsinki, Finland
J. Havukainen, J.K. Heikkilä, T. Järvinen, V. Karimäki, R. Kinnunen, T. Lampén, K. Lassila-Perini, S. Laurila, S. Lehti, T. Lindén, P. Luukka, H. Siikonen, E. Tuominen, J. Tuominiemi

Lappeenranta University of Technology, Lappeenranta, Finland
T. Tuuva

IRFU, CEA, Université Paris-Saclay, Gif-sur-Yvette, France
M. Besancon, F. Couderc, M. Dejardin, D. Denegri, J.L. Faure, F. Ferri, S. Ganjour, S. Ghosh, P. Gras, G. Hamel de Monchenault, P. Jarry, I. Kucher, C. Leloup, E. Locci, M. Machet, J. Malcles, G. Negro, J. Rander, A. Rosowsky, M.Ö. Sahin, M. Titov

Laboratoire Leprince-Ringuet, Ecole polytechnique, CNRS/IN2P3, Université Paris-Saclay, Palaiseau, France
A. Abdulsalam, C. Amendola, I. Antropov, S. Baffioni, F. Beaudette, P. Busson, L. Cadamuro, C. Charlot, R. Granier de Cassagnac, M. Jo, S. Lisniak, A. Lobanov, J. Martin Blanco, M. Nguyen, C. Ochando, G. Ortona, P. Paganini, P. Pigard, R. Salerno, J.B. Sauvan, Y. Sirois, A.G. Stahl Leiton, T. Strebler, Y. Yilmaz, A. Zabi, A. Zghiche

Université de Strasbourg, CNRS, IPHC UMR 7178, F-67000 Strasbourg, France
J.-L. Agram[11], J. Andrea, D. Bloch, J.-M. Brom, M. Buttignol, E.C. Chabert, N. Chanon, C. Collard, E. Conte[11], X. Coubez, J.-C. Fontaine[11], D. Gelé, U. Goerlach, M. Jansová, A.-C. Le Bihan, N. Tonon, P. Van Hove

Centre de Calcul de l'Institut National de Physique Nucleaire et de Physique des Particules, CNRS/IN2P3, Villeurbanne, France
S. Gadrat

Université de Lyon, Université Claude Bernard Lyon 1, CNRS-IN2P3, Institut de Physique Nucléaire de Lyon, Villeurbanne, France
S. Beauceron, C. Bernet, G. Boudoul, R. Chierici, D. Contardo, P. Depasse, H. El Mamouni, J. Fay, L. Finco, S. Gascon, M. Gouzevitch, G. Grenier, B. Ille, F. Lagarde, I.B. Laktineh, M. Lethuillier, L. Mirabito, A.L. Pequegnot, S. Perries, A. Popov[12], V. Sordini, M. Vander Donckt, S. Viret

JHEP08(2018)011

Georgian Technical University, Tbilisi, Georgia
T. Toriashvili[13]

Tbilisi State University, Tbilisi, Georgia
Z. Tsamalaidze[7]

RWTH Aachen University, I. Physikalisches Institut, Aachen, Germany
C. Autermann, L. Feld, M.K. Kiesel, K. Klein, M. Lipinski, M. Preuten, C. Schomakers, J. Schulz, M. Teroerde, V. Zhukov[12]

RWTH Aachen University, III. Physikalisches Institut A, Aachen, Germany
A. Albert, E. Dietz-Laursonn, D. Duchardt, M. Endres, M. Erdmann, S. Erdweg, T. Esch, R. Fischer, A. Güth, M. Hamer, T. Hebbeker, C. Heidemann, K. Hoepfner, S. Knutzen, M. Merschmeyer, A. Meyer, P. Millet, S. Mukherjee, T. Pook, M. Radziej, H. Reithler, M. Rieger, F. Scheuch, D. Teyssier, S. Thüer

RWTH Aachen University, III. Physikalisches Institut B, Aachen, Germany
G. Flügge, B. Kargoll, T. Kress, A. Künsken, T. Müller, A. Nehrkorn, A. Nowack, C. Pistone, O. Pooth, A. Stahl[14]

Deutsches Elektronen-Synchrotron, Hamburg, Germany
M. Aldaya Martin, T. Arndt, C. Asawatangtrakuldee, K. Beernaert, O. Behnke, U. Behrens, A. Bermúdez Martínez, A.A. Bin Anuar, K. Borras[15], V. Botta, A. Campbell, P. Connor, C. Contreras-Campana, F. Costanza, C. Diez Pardos, G. Eckerlin, D. Eckstein, T. Eichhorn, E. Eren, E. Gallo[16], J. Garay Garcia, A. Geiser, J.M. Grados Luyando, A. Grohsjean, P. Gunnellini, M. Guthoff, A. Harb, J. Hauk, M. Hempel[17], H. Jung, M. Kasemann, J. Keaveney, C. Kleinwort, I. Korol, D. Krücker, W. Lange, A. Lelek, T. Lenz, J. Leonard, K. Lipka, W. Lohmann[17], R. Mankel, I.-A. Melzer-Pellmann, A.B. Meyer, G. Mittag, J. Mnich, A. Mussgiller, E. Ntomari, D. Pitzl, A. Raspereza, M. Savitskyi, P. Saxena, R. Shevchenko, N. Stefaniuk, G.P. Van Onsem, R. Walsh, Y. Wen, K. Wichmann, C. Wissing, O. Zenaiev

University of Hamburg, Hamburg, Germany
R. Aggleton, S. Bein, V. Blobel, M. Centis Vignali, T. Dreyer, E. Garutti, D. Gonzalez, J. Haller, A. Hinzmann, M. Hoffmann, A. Karavdina, R. Klanner, R. Kogler, N. Kovalchuk, S. Kurz, T. Lapsien, D. Marconi, M. Meyer, M. Niedziela, D. Nowatschin, F. Pantaleo[14], T. Peiffer, A. Perieanu, C. Scharf, P. Schleper, A. Schmidt, S. Schumann, J. Schwandt, J. Sonneveld, H. Stadie, G. Steinbrück, F.M. Stober, M. Stöver, H. Tholen, D. Troendle, E. Usai, A. Vanhoefer, B. Vormwald

Institut für Experimentelle Kernphysik, Karlsruhe, Germany
M. Akbiyik, C. Barth, M. Baselga, S. Baur, E. Butz, R. Caspart, T. Chwalek, F. Colombo, W. De Boer, A. Dierlamm, N. Faltermann, B. Freund, R. Friese, M. Giffels, M.A. Harrendorf, F. Hartmann[14], S.M. Heindl, U. Husemann, F. Kassel[14], S. Kudella, H. Mildner, M.U. Mozer, Th. Müller, M. Plagge, G. Quast, K. Rabbertz, M. Schröder, I. Shvetsov, G. Sieber, H.J. Simonis, R. Ulrich, S. Wayand, M. Weber, T. Weiler, S. Williamson, C. Wöhrmann, R. Wolf

JHEP08(2018)011

Institute of Nuclear and Particle Physics (INPP), NCSR Demokritos, Aghia Paraskevi, Greece
G. Anagnostou, G. Daskalakis, T. Geralis, A. Kyriakis, D. Loukas, I. Topsis-Giotis

National and Kapodistrian University of Athens, Athens, Greece
G. Karathanasis, S. Kesisoglou, A. Panagiotou, N. Saoulidou

National Technical University of Athens, Athens, Greece
K. Kousouris

University of Ioánnina, Ioánnina, Greece
I. Evangelou, C. Foudas, P. Gianneios, P. Katsoulis, P. Kokkas, S. Mallios, N. Manthos, I. Papadopoulos, E. Paradas, J. Strologas, F.A. Triantis, D. Tsitsonis

MTA-ELTE Lendület CMS Particle and Nuclear Physics Group, Eötvös Loránd University, Budapest, Hungary
M. Csanad, N. Filipovic, G. Pasztor, O. Surányi, G.I. Veres[18]

Wigner Research Centre for Physics, Budapest, Hungary
G. Bencze, C. Hajdu, D. Horvath[19], Á. Hunyadi, F. Sikler, V. Veszpremi

Institute of Nuclear Research ATOMKI, Debrecen, Hungary
N. Beni, S. Czellar, J. Karancsi[20], A. Makovec, J. Molnar, Z. Szillasi

Institute of Physics, University of Debrecen, Debrecen, Hungary
M. Bartók[18], P. Raics, Z.L. Trocsanyi, B. Ujvari

Indian Institute of Science (IISc), Bangalore, India
S. Choudhury, J.R. Komaragiri

National Institute of Science Education and Research, Bhubaneswar, India
S. Bahinipati[21], S. Bhowmik, P. Mal, K. Mandal, A. Nayak[22], D.K. Sahoo[21], N. Sahoo, S.K. Swain

Panjab University, Chandigarh, India
S. Bansal, S.B. Beri, V. Bhatnagar, R. Chawla, N. Dhingra, A. Kaur, M. Kaur, S. Kaur, R. Kumar, P. Kumari, A. Mehta, J.B. Singh, G. Walia

University of Delhi, Delhi, India
A. Bhardwaj, S. Chauhan, B.C. Choudhary, R.B. Garg, S. Keshri, A. Kumar, Ashok Kumar, S. Malhotra, M. Naimuddin, K. Ranjan, Aashaq Shah, R. Sharma

Saha Institute of Nuclear Physics, HBNI, Kolkata, India
R. Bhardwaj, R. Bhattacharya, S. Bhattacharya, U. Bhawandeep, S. Dey, S. Dutt, S. Dutta, S. Ghosh, N. Majumdar, A. Modak, K. Mondal, S. Mukhopadhyay, S. Nandan, A. Purohit, A. Roy, S. Roy Chowdhury, S. Sarkar, M. Sharan, S. Thakur

Indian Institute of Technology Madras, Madras, India
P.K. Behera

JHEP08(2018)011

Bhabha Atomic Research Centre, Mumbai, India

R. Chudasama, D. Dutta, V. Jha, V. Kumar, A.K. Mohanty[14], P.K. Netrakanti, L.M. Pant, P. Shukla, A. Topkar

Tata Institute of Fundamental Research-A, Mumbai, India

T. Aziz, S. Dugad, B. Mahakud, S. Mitra, G.B. Mohanty, N. Sur, B. Sutar

Tata Institute of Fundamental Research-B, Mumbai, India

S. Banerjee, S. Bhattacharya, S. Chatterjee, P. Das, M. Guchait, Sa. Jain, S. Kumar, M. Maity[23], G. Majumder, K. Mazumdar, T. Sarkar[23], N. Wickramage[24]

Indian Institute of Science Education and Research (IISER), Pune, India

S. Chauhan, S. Dube, V. Hegde, A. Kapoor, K. Kothekar, S. Pandey, A. Rane, S. Sharma

Institute for Research in Fundamental Sciences (IPM), Tehran, Iran

S. Chenarani[25], E. Eskandari Tadavani, S.M. Etesami[25], M. Khakzad, M. Mohammadi Najafabadi, M. Naseri, S. Paktinat Mehdiabadi[26], F. Rezaei Hosseinabadi, B. Safarzadeh[27], M. Zeinali

University College Dublin, Dublin, Ireland

M. Felcini, M. Grunewald

INFN Sezione di Bari[a], Università di Bari[b], Politecnico di Bari[c], Bari, Italy

M. Abbrescia[a,b], C. Calabria[a,b], A. Colaleo[a], D. Creanza[a,c], L. Cristella[a,b], N. De Filippis[a,c], M. De Palma[a,b], F. Errico[a,b], L. Fiore[a], G. Iaselli[a,c], S. Lezki[a,b], G. Maggi[a,c], M. Maggi[a], G. Miniello[a,b], S. My[a,b], S. Nuzzo[a,b], A. Pompili[a,b], G. Pugliese[a,c], R. Radogna[a], A. Ranieri[a], G. Selvaggi[a,b], A. Sharma[a], L. Silvestris[a,14], R. Venditti[a], P. Verwilligen[a]

INFN Sezione di Bologna[a], Università di Bologna[b], Bologna, Italy

G. Abbiendi[a], C. Battilana[a,b], D. Bonacorsi[a,b], L. Borgonovi[a,b], S. Braibant-Giacomelli[a,b], R. Campanini[a,b], P. Capiluppi[a,b], A. Castro[a,b], F.R. Cavallo[a], S.S. Chhibra[a], G. Codispoti[a,b], M. Cuffiani[a,b], G.M. Dallavalle[a], F. Fabbri[a], A. Fanfani[a,b], D. Fasanella[a,b], P. Giacomelli[a], C. Grandi[a], L. Guiducci[a,b], S. Marcellini[a], G. Masetti[a], A. Montanari[a], F.L. Navarria[a,b], A. Perrotta[a], A.M. Rossi[a,b], T. Rovelli[a,b], G.P. Siroli[a,b], N. Tosi[a]

INFN Sezione di Catania[a], Università di Catania[b], Catania, Italy

S. Albergo[a,b], S. Costa[a,b], A. Di Mattia[a], F. Giordano[a,b], R. Potenza[a,b], A. Tricomi[a,b], C. Tuve[a,b]

INFN Sezione di Firenze[a], Università di Firenze[b], Firenze, Italy

G. Barbagli[a], K. Chatterjee[a,b], V. Ciulli[a,b], C. Civinini[a], R. D'Alessandro[a,b], E. Focardi[a,b], P. Lenzi[a,b], M. Meschini[a], S. Paoletti[a], L. Russo[a,28], G. Sguazzoni[a], D. Strom[a], L. Viliani[a]

INFN Laboratori Nazionali di Frascati, Frascati, Italy

L. Benussi, S. Bianco, F. Fabbri, D. Piccolo, F. Primavera[14]

INFN Sezione di Genova[a], Università di Genova[b], Genova, Italy

V. Calvelli[a,b], F. Ferro[a], F. Ravera[a,b], E. Robutti[a], S. Tosi[a,b]

JHEP08(2018)011

INFN Sezione di Milano-Bicocca[a], Università di Milano-Bicocca[b], Milano, Italy

A. Benaglia[a], A. Beschi[b], L. Brianza[a,b], F. Brivio[a,b], V. Ciriolo[a,b,14], M.E. Dinardo[a,b], S. Fiorendi[a,b], S. Gennai[a], A. Ghezzi[a,b], P. Govoni[a,b], M. Malberti[a,b], S. Malvezzi[a], R.A. Manzoni[a,b], D. Menasce[a], L. Moroni[a], M. Paganoni[a,b], K. Pauwels[a,b], D. Pedrini[a], S. Pigazzini[a,b,29], S. Ragazzi[a,b], T. Tabarelli de Fatis[a,b]

INFN Sezione di Napoli[a], Università di Napoli 'Federico II'[b], Napoli, Italy, Università della Basilicata[c], Potenza, Italy, Università G. Marconi[d], Roma, Italy

S. Buontempo[a], N. Cavallo[a,c], S. Di Guida[a,d,14], F. Fabozzi[a,c], F. Fienga[a,b], A.O.M. Iorio[a,b], W.A. Khan[a], L. Lista[a], S. Meola[a,d,14], P. Paolucci[a,14], C. Sciacca[a,b], F. Thyssen[a]

INFN Sezione di Padova[a], Università di Padova[b], Padova, Italy, Università di Trento[c], Trento, Italy

P. Azzi[a], N. Bacchetta[a], L. Benato[a,b], D. Bisello[a,b], A. Boletti[a,b], R. Carlin[a,b], A. Carvalho Antunes De Oliveira[a,b], M. Dall'Osso[a,b], P. De Castro Manzano[a], T. Dorigo[a], F. Gasparini[a,b], U. Gasparini[a,b], A. Gozzelino[a], S. Lacaprara[a], P. Lujan, M. Margoni[a,b], A.T. Meneguzzo[a,b], F. Montecassiano[a], N. Pozzobon[a,b], P. Ronchese[a,b], R. Rossin[a,b], F. Simonetto[a,b], E. Torassa[a], M. Zanetti[a,b], P. Zotto[a,b], G. Zumerle[a,b]

INFN Sezione di Pavia[a], Università di Pavia[b], Pavia, Italy

A. Braghieri[a], A. Magnani[a], P. Montagna[a,b], S.P. Ratti[a,b], V. Re[a], M. Ressegotti[a,b], C. Riccardi[a,b], P. Salvini[a], I. Vai[a,b], P. Vitulo[a,b]

INFN Sezione di Perugia[a], Università di Perugia[b], Perugia, Italy

L. Alunni Solestizi[a,b], M. Biasini[a,b], G.M. Bilei[a], C. Cecchi[a,b], D. Ciangottini[a,b], L. Fanò[a,b], R. Leonardi[a,b], E. Manoni[a], G. Mantovani[a,b], V. Mariani[a,b], M. Menichelli[a], A. Rossi[a,b], A. Santocchia[a,b], D. Spiga[a]

INFN Sezione di Pisa[a], Università di Pisa[b], Scuola Normale Superiore di Pisa[c], Pisa, Italy

K. Androsov[a], P. Azzurri[a,14], G. Bagliesi[a], T. Boccali[a], L. Borrello, R. Castaldi[a], M.A. Ciocci[a,b], R. Dell'Orso[a], G. Fedi[a], L. Giannini[a,c], A. Giassi[a], M.T. Grippo[a,28], F. Ligabue[a,c], T. Lomtadze[a], E. Manca[a,c], G. Mandorli[a,c], A. Messineo[a,b], F. Palla[a], A. Rizzi[a,b], A. Savoy-Navarro[a,30], P. Spagnolo[a], R. Tenchini[a], G. Tonelli[a,b], A. Venturi[a], P.G. Verdini[a]

INFN Sezione di Roma[a], Sapienza Università di Roma[b], Rome, Italy

L. Barone[a,b], F. Cavallari[a], M. Cipriani[a,b], N. Daci[a], D. Del Re[a,b,14], E. Di Marco[a,b], M. Diemoz[a], S. Gelli[a,b], E. Longo[a,b], F. Margaroli[a,b], B. Marzocchi[a,b], P. Meridiani[a], G. Organtini[a,b], R. Paramatti[a,b], F. Preiato[a,b], S. Rahatlou[a,b], C. Rovelli[a], F. Santanastasio[a,b]

JHEP08(2018)011

INFN Sezione di Torino[a], Università di Torino[b], Torino, Italy, Università del Piemonte Orientale[c], Novara, Italy

N. Amapane[a,b], R. Arcidiacono[a,c], S. Argiro[a,b], M. Arneodo[a,c], N. Bartosik[a], R. Bellan[a,b], C. Biino[a], N. Cartiglia[a], F. Cenna[a,b], M. Costa[a,b], R. Covarelli[a,b], A. Degano[a,b], N. Demaria[a], B. Kiani[a,b], C. Mariotti[a], S. Maselli[a], E. Migliore[a,b], V. Monaco[a,b], E. Monteil[a,b], M. Monteno[a], M.M. Obertino[a,b], L. Pacher[a,b], N. Pastrone[a], M. Pelliccioni[a], G.L. Pinna Angioni[a,b], A. Romero[a,b], M. Ruspa[a,c], R. Sacchi[a,b], K. Shchelina[a,b], V. Sola[a], A. Solano[a,b], A. Staiano[a], P. Traczyk[a,b]

INFN Sezione di Trieste[a], Università di Trieste[b], Trieste, Italy

S. Belforte[a], M. Casarsa[a], F. Cossutti[a], G. Della Ricca[a,b], A. Zanetti[a]

Kyungpook National University, Daegu, Korea

D.H. Kim, G.N. Kim, M.S. Kim, J. Lee, S. Lee, S.W. Lee, C.S. Moon, Y.D. Oh, S. Sekmen, D.C. Son, Y.C. Yang

Chonbuk National University, Jeonju, Korea

A. Lee

Chonnam National University, Institute for Universe and Elementary Particles, Kwangju, Korea

H. Kim, D.H. Moon, G. Oh

Hanyang University, Seoul, Korea

J.A. Brochero Cifuentes, J. Goh, T.J. Kim

Korea University, Seoul, Korea

S. Cho, S. Choi, Y. Go, D. Gyun, S. Ha, B. Hong, Y. Jo, Y. Kim, K. Lee, K.S. Lee, S. Lee, J. Lim, S.K. Park, Y. Roh

Seoul National University, Seoul, Korea

J. Almond, J. Kim, J.S. Kim, H. Lee, K. Lee, K. Nam, S.B. Oh, B.C. Radburn-Smith, S.h. Seo, U.K. Yang, H.D. Yoo, G.B. Yu

University of Seoul, Seoul, Korea

H. Kim, J.H. Kim, J.S.H. Lee, I.C. Park

Sungkyunkwan University, Suwon, Korea

Y. Choi, C. Hwang, J. Lee, I. Yu

Vilnius University, Vilnius, Lithuania

V. Dudenas, A. Juodagalvis, J. Vaitkus

National Centre for Particle Physics, Universiti Malaya, Kuala Lumpur, Malaysia

I. Ahmed, Z.A. Ibrahim, M.A.B. Md Ali[31], F. Mohamad Idris[32], W.A.T. Wan Abdullah, M.N. Yusli, Z. Zolkapli

JHEP08(2018)011

Centro de Investigacion y de Estudios Avanzados del IPN, Mexico City, Mexico

Duran-Osuna, M. C., H. Castilla-Valdez, E. De La Cruz-Burelo, Ramirez-Sanchez, G., I. Heredia-De La Cruz[33], Rabadan-Trejo, R. I., R. Lopez-Fernandez, J. Mejia Guisao, Reyes-Almanza, R, A. Sanchez-Hernandez

Universidad Iberoamericana, Mexico City, Mexico

S. Carrillo Moreno, C. Oropeza Barrera, F. Vazquez Valencia

Benemerita Universidad Autonoma de Puebla, Puebla, Mexico

J. Eysermans, I. Pedraza, H.A. Salazar Ibarguen, C. Uribe Estrada

Universidad Autónoma de San Luis Potosí, San Luis Potosí, Mexico

A. Morelos Pineda

University of Auckland, Auckland, New Zealand

D. Krofcheck

University of Canterbury, Christchurch, New Zealand

P.H. Butler

National Centre for Physics, Quaid-I-Azam University, Islamabad, Pakistan

A. Ahmad, M. Ahmad, Q. Hassan, H.R. Hoorani, A. Saddique, M.A. Shah, M. Shoaib, M. Waqas

National Centre for Nuclear Research, Swierk, Poland

H. Bialkowska, M. Bluj, B. Boimska, T. Frueboes, M. Górski, M. Kazana, K. Nawrocki, M. Szleper, P. Zalewski

Institute of Experimental Physics, Faculty of Physics, University of Warsaw, Warsaw, Poland

K. Bunkowski, A. Byszuk[34], K. Doroba, A. Kalinowski, M. Konecki, J. Krolikowski, M. Misiura, M. Olszewski, A. Pyskir, M. Walczak

Laboratório de Instrumentação e Física Experimental de Partículas, Lisboa, Portugal

P. Bargassa, C. Beirão Da Cruz E Silva, A. Di Francesco, P. Faccioli, B. Galinhas, M. Gallinaro, J. Hollar, N. Leonardo, L. Lloret Iglesias, M.V. Nemallapudi, J. Seixas, G. Strong, O. Toldaiev, D. Vadruccio, J. Varela

Joint Institute for Nuclear Research, Dubna, Russia

A. Baginyan, A. Golunov, I. Golutvin, V. Karjavin, I. Kashunin, V. Korenkov, G. Kozlov, A. Lanev, A. Malakhov, V. Matveev[35,36], V. Palichik, V. Perelygin, S. Shmatov, N. Skatchkov, V. Smirnov, V. Trofimov, B.S. Yuldashev[37], A. Zarubin

Petersburg Nuclear Physics Institute, Gatchina (St. Petersburg), Russia

Y. Ivanov, V. Kim[38], E. Kuznetsova[39], P. Levchenko, V. Murzin, V. Oreshkin, I. Smirnov, D. Sosnov, V. Sulimov, L. Uvarov, S. Vavilov, A. Vorobyev

JHEP08(2018)011

Institute for Nuclear Research, Moscow, Russia

Yu. Andreev, A. Dermenev, S. Gninenko, N. Golubev, A. Karneyeu, M. Kirsanov, N. Krasnikov, A. Pashenkov, D. Tlisov, A. Toropin

Institute for Theoretical and Experimental Physics, Moscow, Russia

V. Epshteyn, V. Gavrilov, N. Lychkovskaya, V. Popov, I. Pozdnyakov, G. Safronov, A. Spiridonov, A. Stepennov, M. Toms, E. Vlasov, A. Zhokin

Moscow Institute of Physics and Technology, Moscow, Russia

T. Aushev, A. Bylinkin[36]

National Research Nuclear University 'Moscow Engineering Physics Institute' (MEPhI), Moscow, Russia

M. Chadeeva[40], O. Markin, P. Parygin, D. Philippov, S. Polikarpov, V. Rusinov

P.N. Lebedev Physical Institute, Moscow, Russia

V. Andreev, M. Azarkin[36], I. Dremin[36], M. Kirakosyan[36], A. Terkulov

Skobeltsyn Institute of Nuclear Physics, Lomonosov Moscow State University, Moscow, Russia

A. Baskakov, A. Belyaev, E. Boos, V. Bunichev, M. Dubinin[41], L. Dudko, A. Ershov, V. Klyukhin, N. Korneeva, I. Lokhtin, I. Miagkov, S. Obraztsov, M. Perfilov, V. Savrin, P. Volkov

Novosibirsk State University (NSU), Novosibirsk, Russia

V. Blinov[42], D. Shtol[42], Y. Skovpen[42]

State Research Center of Russian Federation, Institute for High Energy Physics, Protvino, Russia

I. Azhgirey, I. Bayshev, S. Bitioukov, D. Elumakhov, A. Godizov, V. Kachanov, A. Kalinin, D. Konstantinov, P. Mandrik, V. Petrov, R. Ryutin, A. Sobol, S. Troshin, N. Tyurin, A. Uzunian, A. Volkov

University of Belgrade, Faculty of Physics and Vinca Institute of Nuclear Sciences, Belgrade, Serbia

P. Adzic[43], P. Cirkovic, D. Devetak, M. Dordevic, J. Milosevic, V. Rekovic

Centro de Investigaciones Energéticas Medioambientales y Tecnológicas (CIEMAT), Madrid, Spain

J. Alcaraz Maestre, A. Álvarez Fernández, I. Bachiller, M. Barrio Luna, M. Cerrada, N. Colino, B. De La Cruz, A. Delgado Peris, C. Fernandez Bedoya, J.P. Fernández Ramos, J. Flix, M.C. Fouz, O. Gonzalez Lopez, S. Goy Lopez, J.M. Hernandez, M.I. Josa, D. Moran, A. Pérez-Calero Yzquierdo, J. Puerta Pelayo, A. Quintario Olmeda, I. Redondo, L. Romero, M.S. Soares

Universidad Autónoma de Madrid, Madrid, Spain

C. Albajar, J.F. de Trocóniz, M. Missiroli

JHEP08(2018)011

Universidad de Oviedo, Oviedo, Spain

J. Cuevas, C. Erice, J. Fernandez Menendez, I. Gonzalez Caballero, J.R. González Fernández, E. Palencia Cortezon, S. Sanchez Cruz, P. Vischia, J.M. Vizan Garcia

Instituto de Física de Cantabria (IFCA), CSIC-Universidad de Cantabria, Santander, Spain

I.J. Cabrillo, A. Calderon, B. Chazin Quero, E. Curras, J. Duarte Campderros, M. Fernandez, J. Garcia-Ferrero, G. Gomez, A. Lopez Virto, J. Marco, C. Martinez Rivero, P. Martinez Ruiz del Arbol, F. Matorras, J. Piedra Gomez, T. Rodrigo, A. Ruiz-Jimeno, L. Scodellaro, N. Trevisani, I. Vila, R. Vilar Cortabitarte

CERN, European Organization for Nuclear Research, Geneva, Switzerland

D. Abbaneo, B. Akgun, E. Auffray, P. Baillon, A.H. Ball, D. Barney, J. Bendavid, M. Bianco, P. Bloch, A. Bocci, C. Botta, T. Camporesi, R. Castello, M. Cepeda, G. Cerminara, E. Chapon, Y. Chen, D. d'Enterria, A. Dabrowski, V. Daponte, A. David, M. De Gruttola, A. De Roeck, N. Deelen, M. Dobson, T. du Pree, M. Dünser, N. Dupont, A. Elliott-Peisert, P. Everaerts, F. Fallavollita, G. Franzoni, J. Fulcher, W. Funk, D. Gigi, A. Gilbert, K. Gill, F. Glege, D. Gulhan, P. Harris, J. Hegeman, V. Innocente, A. Jafari, P. Janot, O. Karacheban[17], J. Kieseler, V. Knünz, A. Kornmayer, M.J. Kortelainen, M. Krammer[1], C. Lange, P. Lecoq, C. Lourenço, M.T. Lucchini, L. Malgeri, M. Mannelli, A. Martelli, F. Meijers, J.A. Merlin, S. Mersi, E. Meschi, P. Milenovic[44], F. Moortgat, M. Mulders, H. Neugebauer, J. Ngadiuba, S. Orfanelli, L. Orsini, L. Pape, E. Perez, M. Peruzzi, A. Petrilli, G. Petrucciani, A. Pfeiffer, M. Pierini, D. Rabady, A. Racz, T. Reis, G. Rolandi[45], M. Rovere, H. Sakulin, C. Schäfer, C. Schwick, M. Seidel, M. Selvaggi, A. Sharma, P. Silva, P. Sphicas[46], A. Stakia, J. Steggemann, M. Stoye, M. Tosi, D. Treille, A. Triossi, A. Tsirou, V. Veckalns[47], M. Verweij, W.D. Zeuner

Paul Scherrer Institut, Villigen, Switzerland

W. Bertl†, L. Caminada[48], K. Deiters, W. Erdmann, R. Horisberger, Q. Ingram, H.C. Kaestli, D. Kotlinski, U. Langenegger, T. Rohe, S.A. Wiederkehr

ETH Zurich - Institute for Particle Physics and Astrophysics (IPA), Zurich, Switzerland

M. Backhaus, L. Bäni, P. Berger, L. Bianchini, B. Casal, G. Dissertori, M. Dittmar, M. Donegà, C. Dorfer, C. Grab, C. Heidegger, D. Hits, J. Hoss, G. Kasieczka, T. Klijnsma, W. Lustermann, B. Mangano, M. Marionneau, M.T. Meinhard, D. Meister, F. Micheli, P. Musella, F. Nessi-Tedaldi, F. Pandolfi, J. Pata, F. Pauss, G. Perrin, L. Perrozzi, M. Quittnat, M. Reichmann, D.A. Sanz Becerra, M. Schönenberger, L. Shchutska, V.R. Tavolaro, K. Theofilatos, M.L. Vesterbacka Olsson, R. Wallny, D.H. Zhu

Universität Zürich, Zurich, Switzerland

T.K. Aarrestad, C. Amsler[49], M.F. Canelli, A. De Cosa, R. Del Burgo, S. Donato, C. Galloni, T. Hreus, B. Kilminster, D. Pinna, G. Rauco, P. Robmann, D. Salerno, K. Schweiger, C. Seitz, Y. Takahashi, A. Zucchetta

JHEP08(2018)011

National Central University, Chung-Li, Taiwan
V. Candelise, Y.H. Chang, K.y. Cheng, T.H. Doan, Sh. Jain, R. Khurana, C.M. Kuo, W. Lin, A. Pozdnyakov, S.S. Yu

National Taiwan University (NTU), Taipei, Taiwan
P. Chang, Y. Chao, K.F. Chen, P.H. Chen, F. Fiori, W.-S. Hou, Y. Hsiung, Arun Kumar, Y.F. Liu, R.-S. Lu, E. Paganis, A. Psallidas, A. Steen, J.f. Tsai

Chulalongkorn University, Faculty of Science, Department of Physics, Bangkok, Thailand
B. Asavapibhop, K. Kovitanggoon, G. Singh, N. Srimanobhas

Çukurova University, Physics Department, Science and Art Faculty, Adana, Turkey
M.N. Bakirci[50], A. Bat, F. Boran, S. Damarseckin, Z.S. Demiroglu, C. Dozen, I. Dumanoglu, S. Girgis, G. Gokbulut, Y. Guler, I. Hos[51], E.E. Kangal[52], O. Kara, U. Kiminsu, M. Oglakci, G. Onengut[53], K. Ozdemir[54], S. Ozturk[50], A. Polatoz, U.G. Tok, H. Topakli[50], S. Turkcapar, I.S. Zorbakir, C. Zorbilmez

Middle East Technical University, Physics Department, Ankara, Turkey
G. Karapinar[55], K. Ocalan[56], M. Yalvac, M. Zeyrek

Bogazici University, Istanbul, Turkey
E. Gülmez, M. Kaya[57], O. Kaya[58], S. Tekten, E.A. Yetkin[59]

Istanbul Technical University, Istanbul, Turkey
M.N. Agaras, S. Atay, A. Cakir, K. Cankocak, I. Köseoglu

Institute for Scintillation Materials of National Academy of Science of Ukraine, Kharkov, Ukraine
B. Grynyov

National Scientific Center, Kharkov Institute of Physics and Technology, Kharkov, Ukraine
L. Levchuk

University of Bristol, Bristol, United Kingdom
F. Ball, L. Beck, J.J. Brooke, D. Burns, E. Clement, D. Cussans, O. Davignon, H. Flacher, J. Goldstein, G.P. Heath, H.F. Heath, L. Kreczko, D.M. Newbold[60], S. Paramesvaran, T. Sakuma, S. Seif El Nasr-storey, D. Smith, V.J. Smith

Rutherford Appleton Laboratory, Didcot, United Kingdom
K.W. Bell, A. Belyaev[61], C. Brew, R.M. Brown, L. Calligaris, D. Cieri, D.J.A. Cockerill, J.A. Coughlan, K. Harder, S. Harper, J. Linacre, E. Olaiya, D. Petyt, C.H. Shepherd-Themistocleous, A. Thea, I.R. Tomalin, T. Williams

Imperial College, London, United Kingdom
G. Auzinger, R. Bainbridge, J. Borg, S. Breeze, O. Buchmuller, A. Bundock, S. Casasso, M. Citron, D. Colling, L. Corpe, P. Dauncey, G. Davies, A. De Wit, M. Della Negra, R. Di

JHEP08(2018)011

Maria, A. Elwood, Y. Haddad, G. Hall, G. Iles, T. James, R. Lane, C. Laner, L. Lyons, A.-M. Magnan, S. Malik, L. Mastrolorenzo, T. Matsushita, J. Nash, A. Nikitenko[6], V. Palladino, M. Pesaresi, D.M. Raymond, A. Richards, A. Rose, E. Scott, C. Seez, A. Shtipliyski, S. Summers, A. Tapper, K. Uchida, M. Vazquez Acosta[62], T. Virdee[14], N. Wardle, D. Winterbottom, J. Wright, S.C. Zenz

Brunel University, Uxbridge, United Kingdom

J.E. Cole, P.R. Hobson, A. Khan, P. Kyberd, I.D. Reid, L. Teodorescu, S. Zahid

Baylor University, Waco, U.S.A.

A. Borzou, K. Call, J. Dittmann, K. Hatakeyama, H. Liu, N. Pastika, C. Smith

Catholic University of America, Washington DC, U.S.A.

R. Bartek, A. Dominguez

The University of Alabama, Tuscaloosa, U.S.A.

A. Buccilli, S.I. Cooper, C. Henderson, P. Rumerio, C. West

Boston University, Boston, U.S.A.

D. Arcaro, A. Avetisyan, T. Bose, D. Gastler, D. Rankin, C. Richardson, J. Rohlf, L. Sulak, D. Zou

Brown University, Providence, U.S.A.

G. Benelli, D. Cutts, A. Garabedian, M. Hadley, J. Hakala, U. Heintz, J.M. Hogan, K.H.M. Kwok, E. Laird, G. Landsberg, J. Lee, Z. Mao, M. Narain, J. Pazzini, S. Piperov, S. Sagir, R. Syarif, D. Yu

University of California, Davis, Davis, U.S.A.

R. Band, C. Brainerd, R. Breedon, D. Burns, M. Calderon De La Barca Sanchez, M. Chertok, J. Conway, R. Conway, P.T. Cox, R. Erbacher, C. Flores, G. Funk, W. Ko, R. Lander, C. Mclean, M. Mulhearn, D. Pellett, J. Pilot, S. Shalhout, M. Shi, J. Smith, D. Stolp, K. Tos, M. Tripathi, Z. Wang

University of California, Los Angeles, U.S.A.

M. Bachtis, C. Bravo, R. Cousins, A. Dasgupta, A. Florent, J. Hauser, M. Ignatenko, N. Mccoll, S. Regnard, D. Saltzberg, C. Schnaible, V. Valuev

University of California, Riverside, Riverside, U.S.A.

E. Bouvier, K. Burt, R. Clare, J. Ellison, J.W. Gary, S.M.A. Ghiasi Shirazi, G. Hanson, J. Heilman, G. Karapostoli, E. Kennedy, F. Lacroix, O.R. Long, M. Olmedo Negrete, M.I. Paneva, W. Si, L. Wang, H. Wei, S. Wimpenny, B. R. Yates

University of California, San Diego, La Jolla, U.S.A.

J.G. Branson, S. Cittolin, M. Derdzinski, R. Gerosa, D. Gilbert, B. Hashemi, A. Holzner, D. Klein, G. Kole, V. Krutelyov, J. Letts, M. Masciovecchio, D. Olivito, S. Padhi, M. Pieri, M. Sani, V. Sharma, M. Tadel, A. Vartak, S. Wasserbaech[63], J. Wood, F. Würthwein, A. Yagil, G. Zevi Della Porta

JHEP08(2018)011

University of California, Santa Barbara - Department of Physics, Santa Barbara, U.S.A.

N. Amin, R. Bhandari, J. Bradmiller-Feld, C. Campagnari, A. Dishaw, V. Dutta, M. Franco Sevilla, L. Gouskos, R. Heller, J. Incandela, A. Ovcharova, H. Qu, J. Richman, D. Stuart, I. Suarez, J. Yoo

California Institute of Technology, Pasadena, U.S.A.

D. Anderson, A. Bornheim, J.M. Lawhorn, H.B. Newman, T. Q. Nguyen, C. Pena, M. Spiropulu, J.R. Vlimant, S. Xie, Z. Zhang, R.Y. Zhu

Carnegie Mellon University, Pittsburgh, U.S.A.

M.B. Andrews, T. Ferguson, T. Mudholkar, M. Paulini, J. Russ, M. Sun, H. Vogel, I. Vorobiev, M. Weinberg

University of Colorado Boulder, Boulder, U.S.A.

J.P. Cumalat, W.T. Ford, F. Jensen, A. Johnson, M. Krohn, S. Leontsinis, T. Mulholland, K. Stenson, S.R. Wagner

Cornell University, Ithaca, U.S.A.

J. Alexander, J. Chaves, J. Chu, S. Dittmer, K. Mcdermott, N. Mirman, J.R. Patterson, D. Quach, A. Rinkevicius, A. Ryd, L. Skinnari, L. Soffi, S.M. Tan, Z. Tao, J. Thom, J. Tucker, P. Wittich, M. Zientek

Fermi National Accelerator Laboratory, Batavia, U.S.A.

S. Abdullin, M. Albrow, M. Alyari, G. Apollinari, A. Apresyan, A. Apyan, S. Banerjee, L.A.T. Bauerdick, A. Beretvas, J. Berryhill, P.C. Bhat, G. Bolla[†], K. Burkett, J.N. Butler, A. Canepa, G.B. Cerati, H.W.K. Cheung, F. Chlebana, M. Cremonesi, J. Duarte, V.D. Elvira, J. Freeman, Z. Gecse, E. Gottschalk, L. Gray, D. Green, S. Grünendahl, O. Gutsche, R.M. Harris, S. Hasegawa, J. Hirschauer, Z. Hu, B. Jayatilaka, S. Jindariani, M. Johnson, U. Joshi, B. Klima, B. Kreis, S. Lammel, D. Lincoln, R. Lipton, M. Liu, T. Liu, R. Lopes De Sá, J. Lykken, K. Maeshima, N. Magini, J.M. Marraffino, D. Mason, P. McBride, P. Merkel, S. Mrenna, S. Nahn, V. O'Dell, K. Pedro, O. Prokofyev, G. Rakness, L. Ristori, B. Schneider, E. Sexton-Kennedy, A. Soha, W.J. Spalding, L. Spiegel, S. Stoynev, J. Strait, N. Strobbe, L. Taylor, S. Tkaczyk, N.V. Tran, L. Uplegger, E.W. Vaandering, C. Vernieri, M. Verzocchi, R. Vidal, M. Wang, H.A. Weber, A. Whitbeck

University of Florida, Gainesville, U.S.A.

D. Acosta, P. Avery, P. Bortignon, D. Bourilkov, A. Brinkerhoff, A. Carnes, M. Carver, D. Curry, R.D. Field, I.K. Furic, S.V. Gleyzer, B.M. Joshi, J. Konigsberg, A. Korytov, K. Kotov, P. Ma, K. Matchev, H. Mei, G. Mitselmakher, K. Shi, D. Sperka, N. Terentyev, L. Thomas, J. Wang, S. Wang, J. Yelton

Florida International University, Miami, U.S.A.

Y.R. Joshi, S. Linn, P. Markowitz, J.L. Rodriguez

Florida State University, Tallahassee, U.S.A.

A. Ackert, T. Adams, A. Askew, S. Hagopian, V. Hagopian, K.F. Johnson, T. Kolberg, G. Martinez, T. Perry, H. Prosper, A. Saha, A. Santra, V. Sharma, R. Yohay

JHEP08(2018)011

Florida Institute of Technology, Melbourne, U.S.A.

M.M. Baarmand, V. Bhopatkar, S. Colafranceschi, M. Hohlmann, D. Noonan, T. Roy, F. Yumiceva

University of Illinois at Chicago (UIC), Chicago, U.S.A.

M.R. Adams, L. Apanasevich, D. Berry, R.R. Betts, R. Cavanaugh, X. Chen, O. Evdokimov, C.E. Gerber, D.A. Hangal, D.J. Hofman, K. Jung, J. Kamin, I.D. Sandoval Gonzalez, M.B. Tonjes, H. Trauger, N. Varelas, H. Wang, Z. Wu, J. Zhang

The University of Iowa, Iowa City, U.S.A.

B. Bilki[64], W. Clarida, K. Dilsiz[65], S. Durgut, R.P. Gandrajula, M. Haytmyradov, V. Khristenko, J.-P. Merlo, H. Mermerkaya[66], A. Mestvirishvili, A. Moeller, J. Nachtman, H. Ogul[67], Y. Onel, F. Ozok[68], A. Penzo, C. Snyder, E. Tiras, J. Wetzel, K. Yi

Johns Hopkins University, Baltimore, U.S.A.

B. Blumenfeld, A. Cocoros, N. Eminizer, D. Fehling, L. Feng, A.V. Gritsan, P. Maksimovic, J. Roskes, U. Sarica, M. Swartz, M. Xiao, C. You

The University of Kansas, Lawrence, U.S.A.

A. Al-bataineh, P. Baringer, A. Bean, S. Boren, J. Bowen, J. Castle, S. Khalil, A. Kropivnitskaya, D. Majumder, W. Mcbrayer, M. Murray, C. Rogan, C. Royon, S. Sanders, E. Schmitz, J.D. Tapia Takaki, Q. Wang

Kansas State University, Manhattan, U.S.A.

A. Ivanov, K. Kaadze, Y. Maravin, A. Mohammadi, L.K. Saini, N. Skhirtladze

Lawrence Livermore National Laboratory, Livermore, U.S.A.

F. Rebassoo, D. Wright

University of Maryland, College Park, U.S.A.

A. Baden, O. Baron, A. Belloni, S.C. Eno, Y. Feng, C. Ferraioli, N.J. Hadley, S. Jabeen, G.Y. Jeng, R.G. Kellogg, J. Kunkle, A.C. Mignerey, F. Ricci-Tam, Y.H. Shin, A. Skuja, S.C. Tonwar

Massachusetts Institute of Technology, Cambridge, U.S.A.

D. Abercrombie, B. Allen, V. Azzolini, R. Barbieri, A. Baty, R. Bi, S. Brandt, W. Busza, I.A. Cali, M. D'Alfonso, Z. Demiragli, G. Gomez Ceballos, M. Goncharov, D. Hsu, M. Hu, Y. Iiyama, G.M. Innocenti, M. Klute, D. Kovalskyi, Y.-J. Lee, A. Levin, P.D. Luckey, B. Maier, A.C. Marini, C. Mcginn, C. Mironov, S. Narayanan, X. Niu, C. Paus, C. Roland, G. Roland, J. Salfeld-Nebgen, G.S.F. Stephans, K. Tatar, D. Velicanu, J. Wang, T.W. Wang, B. Wyslouch

University of Minnesota, Minneapolis, U.S.A.

A.C. Benvenuti, R.M. Chatterjee, A. Evans, P. Hansen, J. Hiltbrand, S. Kalafut, Y. Kubota, Z. Lesko, J. Mans, S. Nourbakhsh, N. Ruckstuhl, R. Rusack, J. Turkewitz, M.A. Wadud

University of Mississippi, Oxford, U.S.A.

J.G. Acosta, S. Oliveros

JHEP08(2018)011

University of Nebraska-Lincoln, Lincoln, U.S.A.

E. Avdeeva, K. Bloom, D.R. Claes, C. Fangmeier, F. Golf, R. Gonzalez Suarez, R. Kamalieddin, I. Kravchenko, J. Monroy, J.E. Siado, G.R. Snow, B. Stieger

State University of New York at Buffalo, Buffalo, U.S.A.

J. Dolen, A. Godshalk, C. Harrington, I. Iashvili, D. Nguyen, A. Parker, S. Rappoccio, B. Roozbahani

Northeastern University, Boston, U.S.A.

G. Alverson, E. Barberis, C. Freer, A. Hortiangtham, A. Massironi, D.M. Morse, T. Orimoto, R. Teixeira De Lima, D. Trocino, T. Wamorkar, B. Wang, A. Wisecarver, D. Wood

Northwestern University, Evanston, U.S.A.

S. Bhattacharya, O. Charaf, K.A. Hahn, N. Mucia, N. Odell, M.H. Schmitt, K. Sung, M. Trovato, M. Velasco

University of Notre Dame, Notre Dame, U.S.A.

R. Bucci, N. Dev, M. Hildreth, K. Hurtado Anampa, C. Jessop, D.J. Karmgard, N. Kellams, K. Lannon, W. Li, N. Loukas, N. Marinelli, F. Meng, C. Mueller, Y. Musienko[35], M. Planer, A. Reinsvold, R. Ruchti, P. Siddireddy, G. Smith, S. Taroni, M. Wayne, A. Wightman, M. Wolf, A. Woodard

The Ohio State University, Columbus, U.S.A.

J. Alimena, L. Antonelli, B. Bylsma, L.S. Durkin, S. Flowers, B. Francis, A. Hart, C. Hill, W. Ji, B. Liu, W. Luo, B.L. Winer, H.W. Wulsin

Princeton University, Princeton, U.S.A.

S. Cooperstein, O. Driga, P. Elmer, J. Hardenbrook, P. Hebda, S. Higginbotham, A. Kalogeropoulos, D. Lange, J. Luo, D. Marlow, K. Mei, I. Ojalvo, J. Olsen, C. Palmer, P. Piroué, D. Stickland, C. Tully

University of Puerto Rico, Mayaguez, U.S.A.

S. Malik, S. Norberg

Purdue University, West Lafayette, U.S.A.

A. Barker, V.E. Barnes, S. Das, S. Folgueras, L. Gutay, M.K. Jha, M. Jones, A.W. Jung, A. Khatiwada, D.H. Miller, N. Neumeister, C.C. Peng, H. Qiu, J.F. Schulte, J. Sun, F. Wang, R. Xiao, W. Xie

Purdue University Northwest, Hammond, U.S.A.

T. Cheng, N. Parashar, J. Stupak

Rice University, Houston, U.S.A.

Z. Chen, K.M. Ecklund, S. Freed, F.J.M. Geurts, M. Guilbaud, M. Kilpatrick, W. Li, B. Michlin, B.P. Padley, J. Roberts, J. Rorie, W. Shi, Z. Tu, J. Zabel, A. Zhang

University of Rochester, Rochester, U.S.A.

A. Bodek, P. de Barbaro, R. Demina, Y.t. Duh, T. Ferbel, M. Galanti, A. Garcia-Bellido, J. Han, O. Hindrichs, A. Khukhunaishvili, K.H. Lo, P. Tan, M. Verzetti

JHEP08(2018)011

The Rockefeller University, New York, U.S.A.
R. Ciesielski, K. Goulianos, C. Mesropian

Rutgers, The State University of New Jersey, Piscataway, U.S.A.
A. Agapitos, J.P. Chou, Y. Gershtein, T.A. Gómez Espinosa, E. Halkiadakis, M. Heindl, E. Hughes, S. Kaplan, R. Kunnawalkam Elayavalli, S. Kyriacou, A. Lath, R. Montalvo, K. Nash, M. Osherson, H. Saka, S. Salur, S. Schnetzer, D. Sheffield, S. Somalwar, R. Stone, S. Thomas, P. Thomassen, M. Walker

University of Tennessee, Knoxville, U.S.A.
A.G. Delannoy, J. Heideman, G. Riley, K. Rose, S. Spanier, K. Thapa

Texas A&M University, College Station, U.S.A.
O. Bouhali[69], A. Castaneda Hernandez[69], A. Celik, M. Dalchenko, M. De Mattia, A. Delgado, S. Dildick, R. Eusebi, J. Gilmore, T. Huang, T. Kamon[70], R. Mueller, Y. Pakhotin, R. Patel, A. Perloff, L. Perniè, D. Rathjens, A. Safonov, A. Tatarinov, K.A. Ulmer

Texas Tech University, Lubbock, U.S.A.
N. Akchurin, J. Damgov, F. De Guio, P.R. Dudero, J. Faulkner, E. Gurpinar, S. Kunori, K. Lamichhane, S.W. Lee, T. Libeiro, T. Mengke, S. Muthumuni, T. Peltola, S. Undleeb, I. Volobouev, Z. Wang

Vanderbilt University, Nashville, U.S.A.
S. Greene, A. Gurrola, R. Janjam, W. Johns, C. Maguire, A. Melo, H. Ni, K. Padeken, P. Sheldon, S. Tuo, J. Velkovska, Q. Xu

University of Virginia, Charlottesville, U.S.A.
M.W. Arenton, P. Barria, B. Cox, R. Hirosky, M. Joyce, A. Ledovskoy, H. Li, C. Neu, T. Sinthuprasith, Y. Wang, E. Wolfe, F. Xia

Wayne State University, Detroit, U.S.A.
R. Harr, P.E. Karchin, N. Poudyal, J. Sturdy, P. Thapa, S. Zaleski

University of Wisconsin - Madison, Madison, WI, U.S.A.
M. Brodski, J. Buchanan, C. Caillol, S. Dasu, L. Dodd, S. Duric, B. Gomber, M. Grothe, M. Herndon, A. Hervé, U. Hussain, P. Klabbers, A. Lanaro, A. Levine, K. Long, R. Loveless, T. Ruggles, A. Savin, N. Smith, W.H. Smith, D. Taylor, N. Woods

†: Deceased
1: Also at Vienna University of Technology, Vienna, Austria
2: Also at IRFU; CEA; Université Paris-Saclay, Gif-sur-Yvette, France
3: Also at Universidade Estadual de Campinas, Campinas, Brazil
4: Also at Universidade Federal de Pelotas, Pelotas, Brazil
5: Also at Université Libre de Bruxelles, Bruxelles, Belgium
6: Also at Institute for Theoretical and Experimental Physics, Moscow, Russia
7: Also at Joint Institute for Nuclear Research, Dubna, Russia
8: Now at Ain Shams University, Cairo, Egypt
9: Now at British University in Egypt, Cairo, Egypt

JHEP08(2018)011

10: Also at Zewail City of Science and Technology, Zewail, Egypt
11: Also at Université de Haute Alsace, Mulhouse, France
12: Also at Skobeltsyn Institute of Nuclear Physics; Lomonosov Moscow State University, Moscow, Russia
13: Also at Tbilisi State University, Tbilisi, Georgia
14: Also at CERN; European Organization for Nuclear Research, Geneva, Switzerland
15: Also at RWTH Aachen University; III. Physikalisches Institut A, Aachen, Germany
16: Also at University of Hamburg, Hamburg, Germany
17: Also at Brandenburg University of Technology, Cottbus, Germany
18: Also at MTA-ELTE Lendület CMS Particle and Nuclear Physics Group; Eötvös Loránd University, Budapest, Hungary
19: Also at Institute of Nuclear Research ATOMKI, Debrecen, Hungary
20: Also at Institute of Physics; University of Debrecen, Debrecen, Hungary
21: Also at Indian Institute of Technology Bhubaneswar, Bhubaneswar, India
22: Also at Institute of Physics, Bhubaneswar, India
23: Also at University of Visva-Bharati, Santiniketan, India
24: Also at University of Ruhuna, Matara, Sri Lanka
25: Also at Isfahan University of Technology, Isfahan, Iran
26: Also at Yazd University, Yazd, Iran
27: Also at Plasma Physics Research Center; Science and Research Branch; Islamic Azad University, Tehran, Iran
28: Also at Università degli Studi di Siena, Siena, Italy
29: Also at INFN Sezione di Milano-Bicocca; Università di Milano-Bicocca, Milano, Italy
30: Also at Purdue University, West Lafayette, U.S.A.
31: Also at International Islamic University of Malaysia, Kuala Lumpur, Malaysia
32: Also at Malaysian Nuclear Agency; MOSTI, Kajang, Malaysia
33: Also at Consejo Nacional de Ciencia y Tecnología, Mexico city, Mexico
34: Also at Warsaw University of Technology; Institute of Electronic Systems, Warsaw, Poland
35: Also at Institute for Nuclear Research, Moscow, Russia
36: Now at National Research Nuclear University 'Moscow Engineering Physics Institute' (MEPhI), Moscow, Russia
37: Also at Institute of Nuclear Physics of the Uzbekistan Academy of Sciences, Tashkent, Uzbekistan
38: Also at St. Petersburg State Polytechnical University, St. Petersburg, Russia
39: Also at University of Florida, Gainesville, U.S.A.
40: Also at P.N. Lebedev Physical Institute, Moscow, Russia
41: Also at California Institute of Technology, Pasadena, U.S.A.
42: Also at Budker Institute of Nuclear Physics, Novosibirsk, Russia
43: Also at Faculty of Physics; University of Belgrade, Belgrade, Serbia
44: Also at University of Belgrade; Faculty of Physics and Vinca Institute of Nuclear Sciences, Belgrade, Serbia
45: Also at Scuola Normale e Sezione dell'INFN, Pisa, Italy
46: Also at National and Kapodistrian University of Athens, Athens, Greece
47: Also at Riga Technical University, Riga, Latvia
48: Also at Universität Zürich, Zurich, Switzerland
49: Also at Stefan Meyer Institute for Subatomic Physics (SMI), Vienna, Austria
50: Also at Gaziosmanpasa University, Tokat, Turkey
51: Also at Istanbul Aydin University, Istanbul, Turkey

JHEP08(2018)011

52: Also at Mersin University, Mersin, Turkey
53: Also at Cag University, Mersin, Turkey
54: Also at Piri Reis University, Istanbul, Turkey
55: Also at Izmir Institute of Technology, Izmir, Turkey
56: Also at Necmettin Erbakan University, Konya, Turkey
57: Also at Marmara University, Istanbul, Turkey
58: Also at Kafkas University, Kars, Turkey
59: Also at Istanbul Bilgi University, Istanbul, Turkey
60: Also at Rutherford Appleton Laboratory, Didcot, United Kingdom
61: Also at School of Physics and Astronomy; University of Southampton, Southampton, United Kingdom
62: Also at Instituto de Astrofísica de Canarias, La Laguna, Spain
63: Also at Utah Valley University, Orem, U.S.A.
64: Also at Beykent University, Istanbul, Turkey
65: Also at Bingol University, Bingol, Turkey
66: Also at Erzincan University, Erzincan, Turkey
67: Also at Sinop University, Sinop, Turkey
68: Also at Mimar Sinan University; Istanbul, Istanbul, Turkey
69: Also at Texas A&M University at Qatar, Doha, Qatar
70: Also at Kyungpook National University, Daegu, Korea

JHEP08(2018)011